

## Crustal evolution and recycling in a juvenile continent: Oxygen isotope ratio of zircon in the northern Arabian Nubian Shield

Yaron Be'eri-Shlevin <sup>a,c,\*</sup>, Yaron Katzir <sup>a</sup>, John W. Valley <sup>b</sup>

<sup>a</sup> Department of Geological and Environmental Sciences, Ben-Gurion University of the Negev, Beer Sheva 84105, Israel

<sup>b</sup> Department of Geology and Geophysics, University of Wisconsin, Madison, Wisconsin 53706, USA

<sup>c</sup> Laboratory for Isotope Geology, Swedish Museum of Natural History, 104 05 Stockholm, Sweden

### ARTICLE INFO

#### Article history:

Received 13 February 2008

Accepted 2 October 2008

Available online 22 October 2008

#### Keywords:

Arabian-Nubian Shield

Oxygen isotopes

Zircon

A-type granites

Magma sources

### ABSTRACT

Crustal recycling patterns during the evolution of the Neoproterozoic Arabian-Nubian Shield (ANS) were defined using the oxygen isotope ratio of zircon [ $\delta^{18}\text{O}(\text{Zrn})$ ]. Evidence for early (~870–740 Ma) crustal recycling in the northernmost ANS (southern Israel and Sinai, Egypt) is given by laser fluorination analysis of bulk zircon separates, which yield higher than mantle  $\delta^{18}\text{O}(\text{Zrn})$  values of several island arc complex (IAC) orthogneisses (6.9 to 8.2‰) and also from the average  $\delta^{18}\text{O}(\text{Zrn})$  value of 6.4‰ determined for detrital zircons (~870–780 Ma) from the Elat-schist; the latter representing the oldest known rock sources in the region. These results indicate prolonged availability of surface-derived rocks for burial or subduction, melting, and assimilation at the very early stages of island arc formation in the ANS. Other IAC intrusions of ~800 Ma show mantle-like  $\delta^{18}\text{O}(\text{Zrn})$  values, implying that not all magmas involved supracrustal contribution. Much younger (650–625 Ma) deformed syn-collisional calc-alkaline (CA1) intrusions are characterized by  $\delta^{18}\text{O}(\text{Zrn})$  values of 5.0 to 7.9‰ indicating continued recycling of the felsic crust.

The main sample set of this study comprises rocks from the mostly granitic, post-collisional calc-alkaline (CA2: ~635–590 Ma) and alkaline (AL: ~608–580 Ma) magmatic suites. Despite having distinct geochemical characteristics and petrogenetic paths and spans of magmatic activity, the two suites are indistinguishable by their average  $\delta^{18}\text{O}(\text{Zrn})$  values of 5.7 and 5.8‰ pointing to the dominance of mantle-like  $\delta^{18}\text{O}$  sources in their formation. Nonetheless, grouping the two suites together reveals geographical zoning in  $\delta^{18}\text{O}(\text{Zrn})$  where a large southeastern region of  $\delta^{18}\text{O}(\text{Zrn})=4.5$  to 5.9‰ is separated from a northwestern belt with  $\delta^{18}\text{O}(\text{Zrn})=6$  to 8‰ by a '6‰ line'.

It is thus suggested that all CA2 and AL magmas of the northernmost ANS were derived from mantle-like  $\delta^{18}\text{O}$  reservoirs in the mafic lower-crust and the lithospheric-mantle, respectively. However, while in the northwestern belt these magmas intruded a thick crustal section and assimilated ~15–35% high- $\delta^{18}\text{O}$  IAC+CA1 material, magmas in the southeastern region intruded a thinner crust and little or no contamination occurred. The proposed NW–SE variance in crustal thickness during the late Neoproterozoic fits well with the geometry of the fan shaped rifting model proposed by Stern [Stern, R.J., 1985. The Najd Fault System, Saudi Arabia and Egypt: a late Precambrian rift related transform system. *Tectonics* 4, 497–511.] for this region. Deep parts of the lithosphere were beginning to rift at ~630 Ma, allowing the asthenospheric mantle to rise and transfer heat to the lithosphere. This resulted in vast melting of the mafic lower-crust to produce the batholithic CA2 magmas. Later (~610 Ma) percolation of lithospheric-mantle melts (possibly along deep seated lithospheric-scale faults) introduced AL magmas to shallow levels of the crust. Intrusion of CA2 and AL mantle-like  $\delta^{18}\text{O}$  parent magmas into the thinned southeastern crust did not involve assimilation of older crust whereas similar intrusion into the thicker northwestern crust resulted in mild assimilation of high- $\delta^{18}\text{O}$  pre-635 Ma crust.

An important implication from our results is that petrogenesis of some high- $\delta^{18}\text{O}$  AL magmas of the northernmost ANS involved assimilation of supracrustal material. Felsic intrusions of the AL suite were previously described as A-type granites derived solely from mantle melts with no crustal components. Our results contribute to the "A-type petrogenesis debate" by showing that their formation can involve recycling of crustal material.

© 2008 Elsevier B.V. All rights reserved.

### 1. Introduction

The Arabian Nubian Shield (ANS) forms one of the largest exposures of juvenile continental crust on earth, comprising

\* Corresponding author.

E-mail address: [aron.beeri@nrm.se](mailto:aron.beeri@nrm.se) (Y. Be'eri-Shlevin).

$\sim 3 \times 10^6 \text{ km}^2$  (Bentor, 1985, Fig. 1, inset). The shield evolved during the Neoproterozoic East African orogeny (900–550 Ma), and is generally viewed as a collage of juvenile volcanic arc terranes and ophiolite remnants that were amalgamated during the assembly of the eastern part of Gondwana (Bentor, 1985; Stern, 1994; Stein and Goldstein, 1996; Stern, 2002; Jarrar et al., 2003; Meert, 2003; Stoesser and Frost, 2006).

The northernmost ANS comprising the northern part of the Eastern Desert of Egypt, Sinai (Egypt), southern Israel and southwestern Jordan (Fig. 1 inset) is characterized by vast and prolonged ( $\sim 820$ –570 Ma) granitoid magmatism. Granitoids were divided to (1) syn- to late-orogenic I-type and (2) post-orogenic, A-type, the transition between the two types occurring at  $\sim 610$ –600 Ma (Beyth et al., 1994; Stern, 1994; Garfunkel, 1999; Jarrar et al., 2003; Moussa et al., 2008). The recognition of a widespread high-K calc-alkaline suite, formed at

about the time of this transition, and partially overlapping the beginning of alkaline A-type magmatism (Be'eri-Shlevin et al., 2009), redefines different stages of calc-alkaline magma production in this region. The magmatic calc-alkaline pulses thus include (a) early medium-K calc-alkaline plutons (now gneisses) associated with metavolcanics and metasediments of island arc complexes (IAC) that formed at  $\sim 820$ –740 Ma, (b) a late syn-collisional medium-K to high-K calc alkaline (CA1) suite formed during late stages of accretion ( $\sim 670$  Ma to 635–625 Ma) and (c) post-collisional mainly high-K calc-alkaline (CA2) suite of 635–590 Ma that overlaps the alkaline (AL) suite of  $\sim 610$  Ma to 580–570 Ma for  $\sim 20$  m.y. The temporal transition from medium-K through high-K calc-alkaline to alkaline magmatism is correlated with the change in tectonic regime (Bentor, 1985; Stern and Hedge, 1985; Beyth et al., 1994; Garfunkel, 1999; Jarrar et al., 2003; Moussa et al., 2008, Be'eri-Shlevin et al., 2009) and implies either a

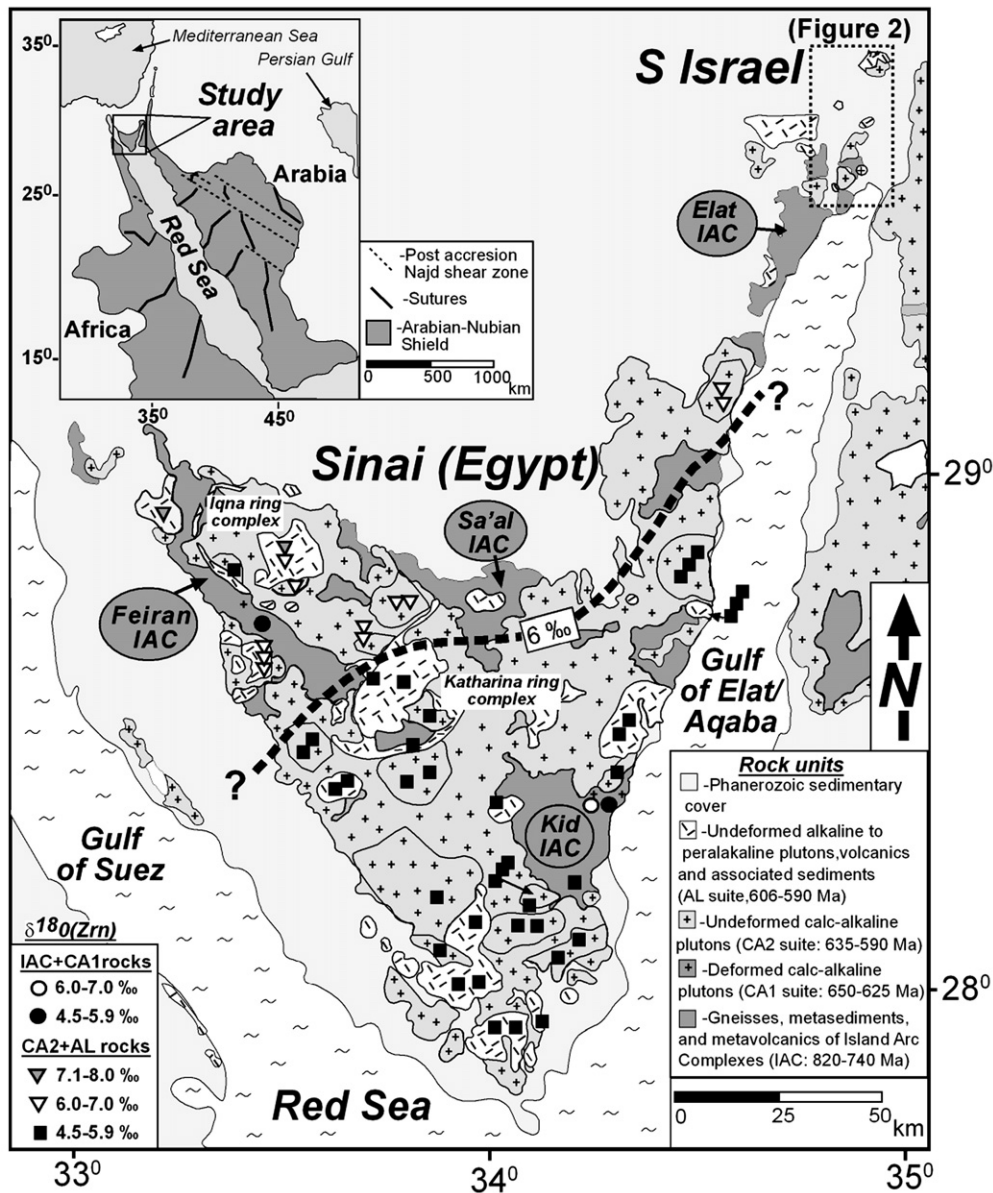


**Fig. 1.** A simplified geological map of the Neoproterozoic ANS exposures in the Sinai Peninsula and southern Israel (after Eyal et al., 1980; Bentor and Eyal, 1987). A dashed rectangle shows the location of Fig. 2. The  $\delta^{18}\text{O}(\text{Zrn})$  of analyzed samples are shown for rocks of all suites (IAC, CA1, CA2, AL). The geographical zoning pattern of  $\delta^{18}\text{O}(\text{Zrn})$  of the joined CA2 and AL suites is marked by a dashed border line (6‰ line) separating a southern zone with mantle-like  $\delta^{18}\text{O}(\text{Zrn})$  vs. a northern belt of mildly higher  $\delta^{18}\text{O}(\text{Zrn})$  values. The location of the large Iqna ring complex and Katharina ring complex are shown. Inset shows the ANS exposures and main suture zones as well as NW–SE post-accretionary faults associated with the Najd system (after Stern, 1985; Hargrove et al., 2006; Stoesser and Frost, 2006). Also shown in inset is the region of the northernmost ANS and the study area in Sinai and southern Israel.

change in magma sources or a change in the processes that formed granitoid magmas during 820–570 Ma. Distinguishing between these two models is complex as both can affect the major and trace element patterns of rocks. Positive  $\epsilon\text{Nd}(T)$  values of +1 to +9 and low Sr; values of  $0.703 \pm 0.002$  measured in rocks of various ages and compositions throughout the shield and average Nd model ages, which overlap earliest crystallization ages were interpreted to represent juvenile crust formation between 900 and 550 Ma with little or no involvement of ancient pre Pan-African continental crust (Bielski, 1982; Stern, 1994; Stein and Goldstein, 1996; Moghazi et al., 1998; Stern, 2002; Jarrar et al., 2003; Mushkin et al., 2003; Hargrove et al., 2006; Katzir et al., 2007b; Moussa et al., 2008). In contrast, there is a growing data base showing that pre Pan African zircons can be found in many ANS intrusions (Sultan et al., 1990; Kennedy et al., 2004; Hargrove et al., 2006; Be'eri-Shlevin et al., 2008). The extent of this pre Pan-African crustal contribution is, however, controversial mainly because in some cases it has almost no effect on the (positive)  $\epsilon\text{Nd}(T)$  of the host rocks (Hargrove et al., 2006). Distinct island arc terranes within the Arabian segment of the shield were inferred by Stoesser and Frost (2006) based on Nd, Pb, Sr and O isotopes, whereas Stein and Goldstein (1996) interpreted the mildly enriched  $\epsilon\text{Nd}(T)$  values to represent derivation of the whole ANS from a mantle-plume.

Regardless of the mode of its generation, either by 'conventional' island arc magmatism and accretion (Bentor, 1985; Stern, 1994; Stoesser and Frost, 2006) or by recycling of an initial plume-derived oceanic plateau (Stein and Goldstein, 1996) the ANS is still considered as juvenile continental crust and thus models referring to its formation must account for its very high crustal production rate (Reymer and Schubert, 1986). One aspect of this problem could be resolved if the ANS includes

more pre Pan-African components then recognized so far as suggested by the inherited zircon patterns. Another important aspect involves recycling within the "juvenile ANS" and identifying when new additions from the mantle to the crust occurred and when and how such young crust was recycled. Using Sr and Nd isotopes to track recycling of young juvenile crust is difficult due to the short residence time of the radiogenic parent species in the crust, resulting in almost constant mantle-like isotope ratios throughout the evolution of the shield. Nevertheless, the abundance of granites throughout the ANS and particularly their predominance in its northernmost part requires efficient recycling process of the initial mantle-derived crust into a felsic, low-density stable continent (Stein, 2003). The oxygen isotope ratio of zircon [ $\delta^{18}\text{O}(\text{Zrn})$ ] has been shown to effectively trace the contribution of young supracrustal material to magma (Peck et al., 2000; Wei et al., 2002; Valley et al., 2005). The asthenospheric mantle is a remarkably homogenous oxygen isotope reservoir (Eiler, 2001) and igneous zircons in high temperature equilibrium with mantle-derived magma have average  $\delta^{18}\text{O}(\text{Zrn}) = 5.3 \pm 0.6\%$  (2SD; Valley et al., 1998). Whole rock  $\delta^{18}\text{O}$  values [ $\delta^{18}\text{O}(\text{WR})$ ] will increase during fractional crystallization of a mafic melt to form a more silicic magma,  $\Delta^{18}\text{O}(\text{WR}-\text{Zrn})$  will change at approximately the same rate such that  $\delta^{18}\text{O}$  of zircon does not change significantly (Valley, 2003). Thus,  $\delta^{18}\text{O}(\text{Zrn})$  can be used to compare sources of variable magmas regardless of their  $\text{SiO}_2$  content. Using the empirical relation  $\delta^{18}\text{O}(\text{WR}) = \delta^{18}\text{O}(\text{Zrn}) + 0.0612 * (\text{SiO}_2 \text{ wt.}\%) - 2.5$  (Valley et al., 2005), (eqn. 1 in this work) and the average  $\text{SiO}_2$ , the  $\delta^{18}\text{O}(\text{Zrn})$  provides an estimate for the  $\delta^{18}\text{O}$  of the magma it crystallized from.

This study uses  $\delta^{18}\text{O}(\text{Zrn})$  to shed light on the sources of the voluminous, mostly granitic magmatism that occurred at the last

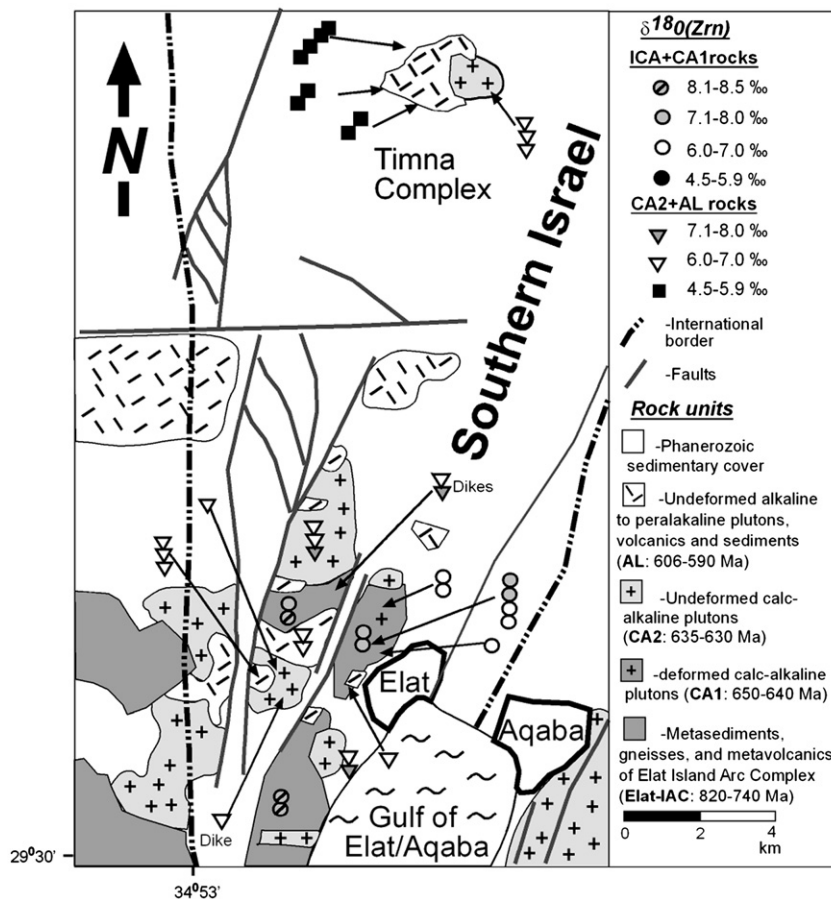


Fig. 2. A simplified geological map of Neoproterozoic exposures in southern Israel (after Eyal et al., 1980; Beyth et al., 1994; Eyal et al., 2004) showing  $\delta^{18}\text{O}(\text{Zrn})$  of analyzed samples. Note that all the area of Fig. 2 is within the higher than mantle  $\delta^{18}\text{O}(\text{Zrn})$  north of the 6‰ line in Fig. 1.

**Table 1**  
Summary of lithological, geochemical, and  $\delta^{18}\text{O}$  data for tectono-magmatic suites in Sinai and southern Israel

Suite	Age (Ma)	Lithology	Geochemical affinity	Assumed setting	$\delta^{18}\text{O}(\text{Zrn})\%$ range (ave.)
Alkaline (AL) suite	610–580	Syenogranites, alkali-feldspar granites and associated dike swarms and volcanics. Minor monzogabbros and monzodiorites	Alkaline to peralkaline, bimodal (mafic felsic), A-type	Attenuation and rifting of the crust	4.5–8.0 (5.8)
Post-collisional batholithic calc-alkaline (CA2) suite	635–590	Granodiorites and monzogranites, some quartz-diorites and minor gabbros	Mostly high-K, metaluminous, and I-type	Post accretion of island arc/continental terranes. Beginning of lithospheric rifting?	5.0–7.2 (5.7)
Late/syn-collisional batholithic calc alkaline (CA1) suite	650–625	Variably deformed quartz-diorites, gabbros, granodiorites and associated intermediate to felsic volcanics	Mostly medium- to high-K, metaluminous to slightly peraluminous and I-type	Late stages of island arc/continental terrane accretion. Subduction still active?	5.0–7.9 (5.8)
Island arc complexes (IAC)	820–740	Metasediments, metavolcanics, migmatites, amphibolites, orthogneisses and paragneisses. All rocks metamorphosed at greenschist to amphibolite facies conditions	Mostly medium-K metaluminous to peraluminous. I-type and S-type (?)	Subduction related island arc formation	5.6–8.2 (6.7)

evolutionary stages of the northernmost ANS in the Sinai Peninsula (Egypt) and southern Israel (Figs. 1 and 2). We present  $\delta^{18}\text{O}(\text{Zrn})$  values for 78 samples representing 41 rock units of the post-collisional calc-alkaline (CA2) and alkaline (AL) magmatic suites. Within Sinai and southern Israel  $\delta^{18}\text{O}(\text{Zrn})$  of these rocks is shown to be geographically zoned, thus revealing an important terrane boundary, here called the “6‰ line”, that separates a large southeastern region of  $\delta^{18}\text{O}(\text{Zrn})=4.5\text{--}5.9\%$  from a northwestern belt with  $\delta^{18}\text{O}(\text{Zrn})=6\text{--}8\%$ . The  $\delta^{18}\text{O}$  provinciality is interpreted in terms variable interaction of mantle-like  $\delta^{18}\text{O}$  parent magmas with the pre-635 Ma crust. To the SE of the 6‰ line magmas evolved from purely mantle-like  $\delta^{18}\text{O}$  derived melts whereas those of the NW of this line were contaminated by supracrustal material. Potential contribution of crustal sources to the post-collisional magmatism is constrained by  $\delta^{18}\text{O}(\text{Zrn})$  values of 9 rock units (represented by 16 samples) from the older metamorphosed suites of pre- to late syn-collisional settings (i.e., IAC and CA1 respectively).

## 2. Geological setting

The basement of the Arabian Nubian Shield (ANS) outcrops along both shores of the Red Sea in NE Africa and W Arabia (Fig. 1, inset). The northernmost ANS in Jordan, Israel, Sinai and the northern part of the Eastern Desert of Egypt (Fig. 1, inset, Fig. 2) includes remnants of deformed island arc complexes (IAC) that are engulfed by voluminous calc-alkaline (CA) batholiths and less voluminous alkaline (AL) plutons, volcanic flows and numerous dike swarms (Fig. 1; Bentor, 1985; Bentor and Eyal, 1987; Garfunkel, 1999; Katzir et al., 2006; Katzir et al., 2007b). A summary of the tectono-magmatic phases in this region is presented in Table 1. In the following sections we briefly describe the rock suites recognized in the northernmost ANS from older to younger, with special emphasis on the exposures in Sinai and southern Israel.

Several IACs were described in the northernmost ANS ranging in age from ~820 Ma to ~740 Ma (U–Pb ages by Stern and Manton, 1987; Kröner et al., 1990; Kröner et al., 1994; El-Shafei and Kusky, 2003; Jarrar et al., 2003 and references therein; Kolodner et al., 2006; Kolodner, 2007). The IACs include migmatites, amphibolites, metapelitic/metapsamitic schists, quartzites, marbles, and basic to intermediate metavolcanics, variably metamorphosed to greenschist or amphibolite facies conditions (Shimron, 1984; Matthews et al., 1989; Katz et al., 1998; El-Shafei and Kusky, 2003 and references therein). The older rock sequences are intruded by mostly medium-K (Fig. 3), metaluminous to peraluminous ( $A/\text{CNK}=0.9\text{--}1.1$ ) tonalites, quartz-diorites, granodiorites and minor high-K monzogranites, all deformed now to gneisses (Stern and Manton, 1987; Eyal et al., 1991; El-Shafei and Kusky, 2003). El-Shafei and Kusky (2003) also describe paragneisses in the Feiran-IAC of western Sinai. Ductile deformation is recorded by all IAC rocks, but the number of deformation events and

their ages are still debated (Eyal, 1980; Shimron, 1984; Eyal et al., 1991; Cosca et al., 1999; El-Shafei and Kusky, 2003). The older and younger IAC sequences and intrusions are thought to represent pre- to syn-collisional tectonic settings, and a subduction-related mechanism for the genesis of their magmas is generally accepted (Bentor, 1985; Stern, 1994; Jarrar et al., 2003; Moussa et al., 2008).

In Sinai and southern Israel three IAC fragmentary pieces (i.e., the Feiran-, Sa'al-, and Elat-IACs) occur along a NE–SW belt (Fig. 1), that is parallel to some of the main sutures detected a few hundred kilometers to the south in Egypt and Saudi Arabia (Stoeser and Camp, 1985; Stern, 1994; Stoeser and Frost, 2006 and references therein; Fig. 1 inset). This NE–SW belt can be traced eastwards into Jordan (Jarrar et al., 2003), but to the west of the Gulf of Suez mainly rocks of younger orogenic phases are described (Stern and Hedge, 1985; Moussa et al., 2008 and references therein). Exposures of the Kid-IAC are located at a more southerly position relative to the major belt of IACs in Sinai (Fig. 1).

The available U–Pb ages in the northernmost ANS imply that batholithic calc-alkaline (CA) magmatism probably commenced not earlier than ~675–650 Ma (Stern and Hedge 1985; Stern and Manton, 1987; Kröner et al., 1990; Eyal et al., 1991; Jarrar et al., 2003; Moussa et al., 2008) terminating a ~70–90 m.y. long lull in magmatic activity following the youngest known island-arc intrusions. Batholithic CA magmatism lasted until 590 Ma (Be'eri-Shlevin et al., 2009), however in the northernmost parts of the ANS this magmatic suite was subdivided by Be'eri-Shlevin et al. (2009) to an older syn to late-collisional ( $\geq 635\text{--}625$  Ma) suite (CA1) and a younger ( $\leq 635$  Ma) post-collisional suite (CA2). In this area penetrative ductile deformation is

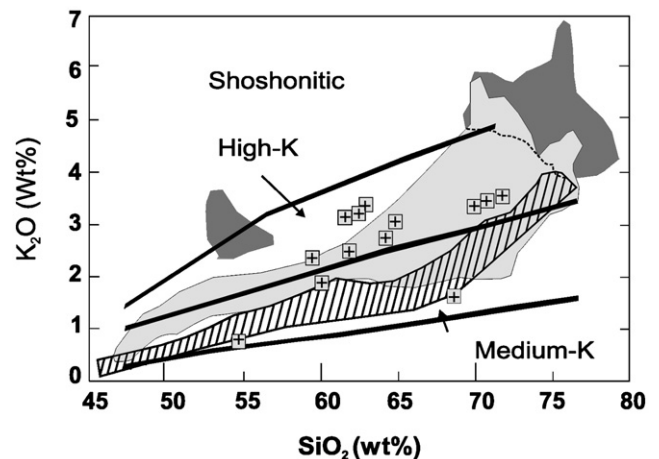


**Fig. 3.**  $\text{K}_2\text{O}$  vs.  $\text{SiO}_2$  (wt.%) for rocks of Sinai and southern Israel after Be'eri-Shlevin et al. (2009). IAC: diagonally lined; CA1: crosses; CA2: light gray; AL: dark gray. Values for IAC rocks are from our own unpublished analyses.

recorded only in rocks predating ~635–625 Ma which is also the time of terminal collision and the end of subduction in this region (Katz et al., 2004; Be'eri-Shlevin et al., 2009). In the more central parts of the ANS (southern and central parts of the Eastern Desert of Egypt and in Arabia) ductile deformation probably associated with activity along the Najd fault system, continued much later (Greiling et al., 1994; Andersen et al., *in press*). The 650–625 Ma CA1 intrusions from Sinai and southern Israel generally show evidence of ductile deformation in the form of aligned mafic minerals but with no mesoscale layering and no evidence of high-T metamorphism. These rocks are defined here as deformed granitoids/plutons in order to avoid ambiguity with the gneisses of the older IACs. The CA suite (CA1+CA2) of Sinai and southern Israel spans a full range of mafic to felsic plutons ( $\text{SiO}_2=45\text{--}75$  wt.%), the latter being dominant. Plutons of this suite span metaluminous to peraluminous compositions ( $A/\text{CNK}=0.7\text{--}1.2$ ), but minor strongly peraluminous plutons also occur (Be'eri-Shlevin et al., 2009). Intermediate to mafic plutons are quartz-diorites and minor gabbros. The more dominant felsic plutons are granodiorites and monzogranites with minor monzonites and quartz monzonites. While syn-collisional (CA1) plutons are medium-K to high-K, the post-collisional plutons especially of intermediate to felsic composition are generally high-K (Fig. 3) (Bentor and Eyal, 1987; Moghazi et al., 1998; Eyal et al., 2004; Be'eri-Shlevin et al., 2009).

A transition to alkaline magmatism in the northernmost ANS occurred along with a shift in tectonics to an extensional regime (Bentor, 1985; Stern and Hedge, 1985; Beyth et al., 1994; Stern 1994; Garfunkel, 1999; Jarrar et al., 2003). Rocks of the AL suite include alkaline to peralkaline (Na-amphibole bearing) felsic ( $\text{SiO}_2: 70\text{--}79$  wt.%) and rare mafic and intermediate plutons, as well as bimodal (mafic-felsic) alkaline and peralkaline volcanic rocks and dike swarms (Katzir et al., ; Bentor, 1985; Bentor and Eyal, 1987; Beyth et al., 1994; Moghazi et al., 1998; Garfunkel, 1999; Katzir et al., 2006; 2007a,b). Plutonic rocks are generally syenogranites and alkali feldspar granites, but a few monzogabbros and a monzodiorite intrusion (e.g., Beyth et al., 1994) were identified (Table 1). Volcanic and dike rocks include rhyolites, trachydolerites, quartz-syenites, and monzonites (Jarrar et al., 2003; Katzir et al., 2007a,b). The bimodal (mafic-felsic) character of this suite is also expressed by abundant composite dikes with felsic interiors and mafic margins (Jarrar et al., 2004; Katzir et al., 2007b). Several authors discussed the timing of the transition to alkaline magmatism in the northern ANS (Beyth et al., 1994; Stern, 1994; Garfunkel, 1999; Jarrar et al., 2003). Recent ion microprobe U–Pb dating compiled with previously published TIMS U–Pb data has shown that AL magmatism spans a time range of ~610–580 Ma (Andersen et al., *in press*; Moussa et al., 2008; Be'eri-Shlevin et al., 2009). Importantly it has been shown that the end of CA2 magmatism overlaps with the beginning of AL magmatism, and thus in the same tectonic setting both magma types were produced (Be'eri-Shlevin et al., 2009). Rocks of the CA (1+2) and AL suites in southern Israel and Sinai generally correlate with the Aqaba and Araba suites of southwestern Jordan, respectively (Jarrar et al., 2003), and with Granite I+II and Granite III of eastern Egypt (Eyal et al., 2004 and references therein).

A prominent feature of the northernmost ANS is the lack of evidence for activity of the post-accretionary NW–SE trending faults of the Najd system (Fig. 1, inset) detected further south in the Central Eastern Desert of Egypt and in Arabia (Stern, 1985). Activity along the Najd fault system was associated with ductile and brittle deformation, but no displacement associated with inferred northerly extensions of such faults into the northern part of the Eastern Desert of Egypt, Sinai, southern Israel or southwestern Jordan can be traced. Ductile deformation in these parts of the ANS is recorded only in rocks predating ~625 Ma. These features point to a very different tectono-magmatic evolution in the northernmost ANS vs. more southerly segments of ANS after ~625 Ma (Stern, 1985; Stern and Hedge, 1985; Be'eri-Shlevin et al., 2009).

### 3. Sample description

Our sampling consists mainly of rocks from the CA2 and AL suites in Sinai and southern Israel. These rocks postdate the main ductile penetrative deformation events in this segment of the northern ANS ( $\leq 635\text{--}625$  Ma). Samples were chosen to provide good geographical coverage and represent the full variety of geochemical composition within these suites. In most cases (>80%) two or more samples of the same pluton/dike were analyzed representing its compositional variance if any, and especially in the case of large plutons their geographical exposure (Appendix A).

The CA2 suite is represented here by plutonic rocks varying from an amphibole bearing gabbro through amphibole-biotite bearing quartz-diorites and granodiorites to biotite bearing monzogranite (Figs. 1 and 2, Tables 1 and 2). These are medium to coarse grained rocks that in many cases host abundant micro-granular mafic enclaves of dioritic composition. Several complex bodies within this suite were sampled: a layered gabbro-diorite pluton and several zoned granitoids of quartz-diorite to granodiorite and monzogranite compositions (Bentor and Eyal, 1987, Table 1). Samples from the AL suite consist of dikes, sub-volcanic bodies and plutons. Plutonic rocks were sampled both in southern Israel and in Sinai, and include medium to coarse grained biotite bearing syenogranites, biotite or amphibole-biotite bearing alkali feldspar granites, Na-amphibole bearing alkali feldspar granites, and minor pyroxene-amphibole bearing monzogabbro and monzodiorite intrusions. Enclaves are rare to absent in these rocks. The large (150–200 km<sup>2</sup>, Table 2) Iqna and Katharina granite plutons in Sinai form the central part of volcanic ring complexes (Fig. 1; Katzir et al., 2007a). The Katharina quartz-syenite ring dike and the Iqna sub-volcanic monzonitic rocks, intruded by the syenogranite/alkali feldspar granites, were also sampled. Several alkaline rhyolitic (quartz porphyry) dikes (some forming interior parts of composite dikes) and sub-volcanic bodies were sampled in southern Israel (Fig. 2; Katzir et al., 2007b).

Zircons of the CA2 and AL suites are yellowish to pink, euhedral, and generally show simple oscillatory magmatic zoning and minor sector zoning in CL and SE images (Fig. 4f–h). Recent ion-microprobe dating of zircons from more than 35 representative CA2 and AL plutons and dikes has shown that inheritance is very minor in both suites (Be'eri-Shlevin et al., 2009, Be'eri-Shlevin unpublished U–Pb ion-microprobe dating). Unambiguously xenocrystic zircons were detected only in three out of the 35 plutons and dykes for which the bulk  $\delta^{18}\text{O}(\text{Zrn})$  is reported here (Be'eri-Shlevin et al., 2009). Two of them are the small (1–3 km<sup>2</sup>) intrusions of the Elat-granite (Elat-Sholomo and Elat-Rehavim in Table 2, Appendix A; see also Eyal et al., 2004), the third is the zoned Zreir pluton (~100 km<sup>2</sup>) of quartz-diorite to granodiorite and monzogranite composition (Table 2, Appendix A). In both the Elat-granites and the Zreir pluton, xenocrystic zircon comprises only a small component within the zircon population, manifesting the minor inheritance characteristic of the CA2 and AL suites (Be'eri-Shlevin et al., 2009).

In addition to the samples of the CA2 and AL suites, 11 samples representing 5 rock units of the IACs (~870–740 Ma) and 5 samples representing 4 rock units of the CA1 suite (~650–625 Ma) were also analyzed for  $\delta^{18}\text{O}(\text{Zrn})$ . This sample set, albeit small compared to those of the younger (CA2+AL) magmatic suites, provides preliminary insight into the temporal variation of  $\delta^{18}\text{O}$  throughout the earlier evolution of the northernmost ANS (820–625 Ma). Sampled IAC rocks include: (a) meta-sediments of pelitic to psammitic composition [Elat schist (~820 Ma, Kröner et al., 1990; Kolodner et al., 2006; Kolodner, 2007), Fig. 1, Table 2]; (b) a paragneiss [Aliat paragneiss (~800 Ma; Be'eri-Shlevin, 2008), Fig. 1, Table 2] from the Feiran-IAC which is similar in mineralogy and age to the banded paragneisses described by Stern and Manton (1987) and El-Shafei and Kusky (2003); (c) three intermediate to felsic orthogneisses of ~780–740 Ma (Kröner et al., 1990) that intrude the Elat schist. The latter are medium to coarse-grained amphibole-biotite bearing orthogneisses of tonalite to quartz-

**Table 2**  
 $\delta^{18}\text{O}(\text{Zrn})$  values for rocks of the northern ANS in Sinai and southern Israel

No. <sup>a</sup>	Rock	Surface ex. (km <sup>2</sup> )	Age <sup>b</sup> (Ma)	SiO <sub>2</sub> (ave) wt.%	Suite	Lithology	Zircons <sup>c</sup>	$\delta^{18}\text{O}(\text{Zrn})$	n <sup>d</sup>	1 $\sigma$ <sup>e</sup>	$\delta^{18}\text{O}(\text{WR})$ <sup>f</sup>
1	Elat schist	7	870–780 (820) <sup>1</sup>		Elat-IAC	Metapsammitic/pelitic sediments	Det	6.41	2	0.10	
2	Taba orthogneiss	10	780±10 <sup>2</sup>	68	Elat-IAC	Tonalite	Mag, min. xen?	8.09	2	0.00	9.75
3	Roded orthogneiss	2	780	62	Elat-IAC	Qtz-diorite to granodiorite	Mag	8.18	2	0.20	9.47
4	Elat granitic orthogneiss	15	740±10 <sup>2</sup>	75	Elat-IAC	Monzogranite	Mag	6.92	4	0.30	9.01
5	Aliat paragneiss	15	803±9 <sup>3</sup>	70	Feiran-IAC	Granodiorite (metasediments?)	Mag/det ?	5.57	1	0.04	7.35
6	SMGD def. pluton	2	650–640 <sup>2</sup>	55	CA1	Gabbro to diorite	Mag	7.32	2	0.10	8.19
7	SGG def. pluton	1	640±9	74	CA1	Monzogranite	Mag	7.93	1	0.10	9.96
8	Jantil def. pluton	40	622±3 <sup>3</sup>	69	CA1	Monzogranite	Mag	6.57	1	0.01	8.29
9	Rurabi def. pluton	40	632±4 <sup>3</sup>	60	CA1	Quartz-diorite	Mag	4.99	1	0.03	6.16
10	Elat-Shlomo pluton	2	636±8 <sup>4</sup>	75	CA2	Monzogranite	Mag, min. xen	7.06	1	0.09	9.15
11	Elat-Rehavam pluton	2	630±5 <sup>4</sup>	73	CA2	Monzogranite	Mag, min. xen	6.36	2	0.03	8.33
12	RQD pluton	10	634±2 <sup>5</sup>	62	CA2	Quartz-diorite	Mag	6.61	3	0.39	7.90
13	TPG pluton	2	632±7 <sup>4</sup>	70	CA2	Monzogranite (porphyritic)	Mag	6.17	3	0.10	7.95
14	Shahira pluton	45	632±4 <sup>4</sup>	55	CA2	Gabbro-diorite layered intrusion	Mag	5.43	1	0.11	6.30
15	Zreir pluton	100	629±6 <sup>4</sup>	65	CA2	Monzodiorite to monzogranite	Mag, min. xen	5.32	3	0.39	6.80
16	Hibran-Miar pluton	80	619±4 <sup>4</sup>	60	CA2	Monzodiorite to monzogranite	Mag	5.45	2	0.24	6.62
17	Rahba pluton	100	610±5 <sup>4</sup>	68	CA2	Monzogranite to Qtz-monzonite	Mag	5.69	2	0.10	7.35
18	Ahdar pluton	150	610±5 <sup>4</sup>	67	CA2	Granodiorite to monzogranite	Mag	6.50	2	0.01	8.10
19	Sama pluton	20	608±4 <sup>4</sup>	66	CA2	Monzogranite to Qtz-monzonite	Mag	5.14	3	0.09	6.68
20	Lathi pluton	170	607±4 <sup>4</sup>	72	CA2	Monzogranite to Qtz-monzonite	Mag	5.05	2	0.02	6.96
21	Malaha pluton	100	605±4 <sup>4</sup>	61	CA2	Quartz-diorite to monzonite	Mag, min. xen?	6.77	2	0.11	8.00
22	Girgar pluton	200	603±4 <sup>4</sup>	72	CA2	Monzo/syenogranite	Mag	5.30	1	0.14	7.21
23	Gashi pluton	80	600	70	CA2	Monzogranite	Mag	5.16	1	0.10	6.94
24	Mandar pluton	150	604±4 <sup>6</sup>	74	CA2	Monzogranite	Mag	5.28	2	0.01	7.31
25	Sulaf pluton	100	597±5 <sup>4</sup>	66	CA2	Monzogranite to monzonite	Mag	6.14	2	0.04	7.68
26	Abu-K'sheib pluton	80	592±7 <sup>4</sup>	67	CA2	Quartz-monzonite (porphyritic)	Mag, min. xen?	5.25	1	0.01	6.85
27	Tubeina pluton	80	600	74	CA2	Monzogranite	Mag	6.50	1	0.10	8.53
28	Nasrin pluton	40	599±5 <sup>3</sup>	50	AL	Monzogabbro	Mag	5.89	1	0.10	6.45
29	TAG pluton	2	606±3 <sup>4</sup>	75	AL	A-fel granite	Mag	5.50	2	0.02	7.59
30	TMN pluton	2	602±5 <sup>4</sup>	53	AL	Monzodiorite	Mag	5.78	4	0.16	6.52
31	Timna syenite pluton	<1	603	60	AL	Syenite	Mag	5.79	2	0.03	6.96
32	Yehoshafat pluton	2	605±4 <sup>4</sup>	75	AL	A-fel granite	Mag	6.63	3	0.12	8.72
33	Elat subvolcanics	<1	595	75	AL	Rhyolite (Qtz-porphyry)	Mag	6.49	1	0.10	8.58
34	Elat composite dike	<1	590±9 <sup>6</sup>	75	AL	Rhyolite (Qtz-porphyry)	Mag	6.84	2	0.39	8.93
35	Elat rhyolite dike1	<1	595	75	AL	Rhyolite	Mag	6.36	1	0.10	8.45
36	Elat rhyolite dike2	<1	600±8 <sup>6</sup>	75	AL	Rhyolite	Mag	6.35	1	0.10	8.44
37	Elat rhyolite dike3	<1	588±10 <sup>6</sup>	75	AL	Rhyolite	Mag	6.23	1	0.10	8.32
38	Sahara pluton	210	608±5 <sup>4</sup>	75	AL	Na-amph A-fel granite	Mag	5.14	3	0.05	7.23
39	Sharm pluton	150	594±4 <sup>4</sup>	72	AL	A-fel granite	Mag	4.79	3	0.16	6.70
40	Yahmed pluton	10	595	70	AL	Syenogranite	Mag	4.49	1	0.10	6.27
41	Umm-Shomer pluton	80	596±5 <sup>4</sup>	73	AL	Syenogranite	Mag	5.13	2	0.12	7.10
42	Dahab pluton	100	591±6 <sup>4</sup>	70	AL	Syenogranite	Mag	5.20	2	0.14	6.98
43	Serbal pluton	100	611±7 <sup>3</sup>	74	AL	A-fel granite	Mag	6.70	3	0.20	8.73
44	Umm-I-Fai pluton	10	586±4 <sup>4</sup>	73	AL	Na-amph A-fel granite	Mag	5.49	3	0.09	7.46
45	Iqna-Kid pluton	50	600	73	AL	A-fel granite	Mag	5.65	1	0.02	7.62
46	Umm-Bugma pluton	80	597±5 <sup>3</sup>	75	AL	Syenogranite	Mag	8.04	1	0.10	10.13
47	Katharina ring dikes	40	590	65	AL	Syenite (Qtz-porphyry)	Mag	5.53	4	0.09	7.01
48	Katharina pluton	200	583±6 <sup>4</sup>	76	AL	Syenogranite	Mag	5.82	1	0.06	7.97
49	Iqna subvolcanics	30	590	65	AL	Qtz-monzonite (Qtz-porphyry)	Mag	6.68	1	0.05	8.16
50	Iqna pluton	150	578±8 <sup>4</sup>	76	AL	Syenogranite	Mag	7.07	1	0.10	9.22

Abbreviations for rock suites: IAC – Island Arc Complex (deformed), CA1 – Batholithic calc-alkaline 1 suite (deformed), CA2 – Batholithic calc-alkaline 2 suite (undeformed), AL – Alkaline suite (undeformed). Other abbreviations: A-fel: alkali feldspar, Def: deformed; ex: exposure, Mag: magmatic, Det: detrital, Na-amph: Na-amphibole, Qtz-quartz, SGG: Shahmon gneissic granite (e.g., Eyal et al., 2004), SMGD: Shahmon Metagabbro/diorite (e.g., Eyal et al., 1991) TAG: Timna alkali granite, TMN: Timna monzodiorite, TPG: Timna porphyritic granite, Xen: xenocrysts.

<sup>a</sup>Sample location is found in Appendices A and B.

<sup>b</sup>Normal text: U–Pb ages from (1 – Kolodner et al., 2006; 2 – Kröner et al., 1990, 3 – Be'eri-Shlevin unpublished ion-microprobe data; 4 – Be'eri-Shlevin et al., 2009; 5 – Katz et al., 1998; 6 – Be'eri-Shlevin, 2008). Underlined text: Rb–Sr age (from Eyal et al., 2004). Text in italics: age estimate based on field relations with dated rocks. All reported age uncertainties are 2 $\sigma$ .

<sup>c</sup>Interpretation of zircon origin (magmatic vs. detrital) and characteristics (xenocryst bearing vs. only magmatic population) based on U–Pb dating, CL images and other considerations.

<sup>d</sup>n = number of different rock samples (representing compositional and/or geographical variance) used for determining the average  $\delta^{18}\text{O}(\text{Zrn})$ .

<sup>e</sup>In cases where only one rock sample was analyzed and no duplicate aliquots were analyzed from this sample a  $\pm 0.1\%$  internal error (1 $\sigma$ ) was assigned to the rock value. In cases where one rock sample was used but duplicate aliquots analyzed the corresponding error (1 $\sigma$ ) was used.

<sup>f</sup> $\delta^{18}\text{O}(\text{WR})$  calculated using eqn. 1 from Valley et al. (2005) and the average SiO<sub>2</sub> content.

diorite and granodiorite in composition and a biotite bearing monzogranite orthogneiss (Fig. 2, Table 2). Sampled CA1 rocks include: (a) pyroxene-amphibole bearing metagabbro/diorite [Shahmon Metagabbro/diorite (~650–640 Ma, U–Pb age) of Kröner et al., 1990; Fig. 2, Table 2]; (b) a deformed biotite bearing monzogranite (Shahmon gneissic granite (~640 Ma, Rb–Sr age) of Eyal et al., 2004; Fig. 2, Table 2); (c) a deformed amphibole-biotite bearing quartz-

diorite (Rurabi pluton, Fig. 1, Table 2); and (d) a deformed, amphibole-biotite bearing, granodiorite (Jantil pluton, Fig. 1, Table 2). The latter two plutons were dated to ~630–625 Ma (Be'eri-Shlevin unpublished U–Pb ion-microprobe data).

Zircons of IAC and CA1 rocks are yellowish to pink. Detrital zircons of the Elat schist (of the Elat-IAC) are variably rounded although the majority of this population shows only slightly rounded to euhedral

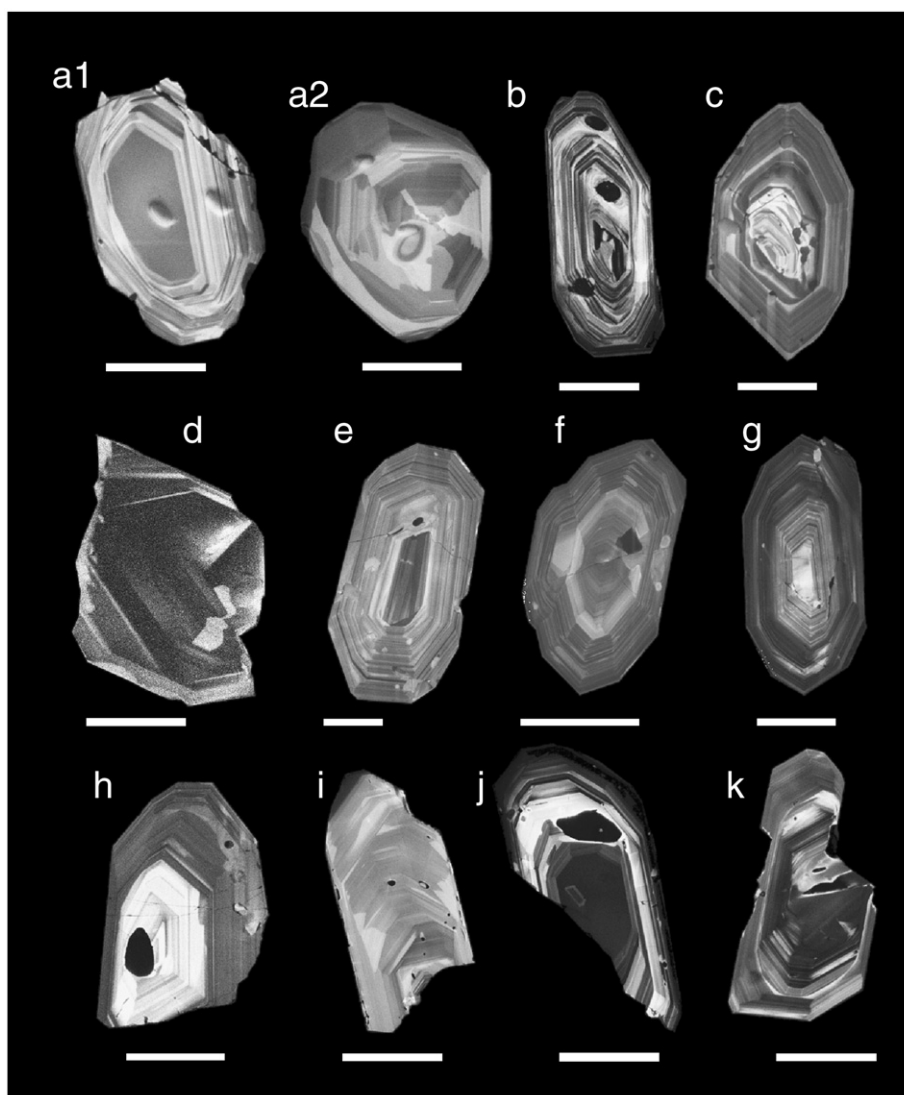


**Fig. 4.** Representative cathodoluminescence (CL) images of zircons from some of the analyzed rocks in this study. IAC-rocks: (a1,2) Elat schist: detrital zircons showing variable rounded (to unrounded) edges, (b) Aliat paragneiss (c) Taba orthogneiss; CA1-rocks (d) Shahmon metagabbro/diorite, (e) Jantil deformed pluton, CA2-rocks: (f) Zreir pluton, (g) Ahdar pluton, (h) Lathi pluton; AL-rocks: (i) Sharm pluton, (j) Katharina pluton, (k) Composite dikes: quartz-porphry interior. Scale bars are 100  $\mu\text{m}$ . For details see text.

features (Fig. 4a1 and a2). Zircons from gneisses and deformed granitoids are all euhedral (Fig. 4b–e). The rocks of the IAC and CA1 suites have experienced a more complex history than CA2 and AL rocks thus the occurrence or lack of zircon inheritance or metamorphic overgrowths were carefully determined before multi-grain analysis. Metamorphic zircon overgrowths can be distinguished by low Th/U ratios ( $<0.2$ ) and dark non-oscillatory zoned rims (Hoskin and Schaltegger, 2003; Cavosie et al., 2006). Inheritance may be indicated either by CL imaging or by in-situ dating of zircon core domains. Zircons from all IAC+CA1 sampled rocks (schists, gneisses and deformed plutons) show simple oscillatory magmatic zoning in CL with some sector zoning, except for rare cases where older cores are suspected (i.e., cross cutting relations between core and rim areas, Fig. 4c). Darker rims are seen in the CL images of zircons from some samples (Fig. 4a2 and b), however the remnants of igneous oscillatory zoning in these domains and SIMS dating which yields the same age for bright cores and darker rims (Kolodner, 2007; Be'eri-Shlevin unpublished U–Pb ion-microprobe data) are taken as evidence that they do not represent metamorphic overgrowths.

Special attention was paid to inspect the age range and U–Th–Pb characteristics of the detrital zircons of the Elat-schist. Earlier U–Pb

age determinations have shown that the Elat schist zircons range from 870 to 780 Ma, but cluster around 820 Ma (U–Pb single zircon evaporation ages: Kröner et al., 1990; U–Pb SHRIMP dating: Kolodner et al., 2006; Kolodner, 2007). Recent ion microprobe dating of representative zircons from the same zircon separate analyzed for bulk  $\delta^{18}\text{O}(\text{Zrn})$  in this work, has yielded similar results although with a more restricted age range around 820 Ma (Be'eri-Shlevin unpublished U–Pb ion-microprobe data). The age range and oscillatory zoning in CL images (Fig. 4a1 and a2) as well as the Th/U ratios of these analyses (0.23–0.83; average: 0.51) suggests a magmatic origin of these zircons with no evidence of metamorphic overgrowths (Hoskin and Schaltegger, 2003; Cavosie et al., 2006).

#### 4. Analytical methods

Zircon was extracted from 1–10 kg crushed samples using standard methods, including a Wilfley shaking table and separation by heavy liquids. The least magnetic zircon fractions were isolated using a Frantz isodynamic magnetic separator operated at a side tilt of 4 to 5°. Final purification from the 63–300  $\mu\text{m}$  size fraction included hand picking under a binocular microscope. Zircon concentrates were treated with a

series of cold acids ( $\text{HNO}_3$ ,  $\text{HCl}$ , and  $\text{HF}$ ) to remove potential contaminants. Importantly, treating the samples with cold  $\text{HF}$  removes not only external contaminants (grain boundaries, inclusions), but also any possible metamict zircon domains that might be subject to post-magmatic oxygen isotope exchange (Valley, 2003). Zircon aliquots (1.5–3 mg) were crushed using a boron-carbide mortar and pestle to limit grain size effects and to maximize fluorination efficiency during lasing.

Oxygen isotope analyses were performed using the laser fluorination technique at the University of Wisconsin, Madison (Valley et al., 1995).  $\text{BrF}_5$  was used as the reagent. Oxygen was purified cryogenically and with an inline Hg diffusion pump, converted to  $\text{CO}_2$  using a hot graphite rod and analyzed on a Finnigan MAT 251 mass spectrometer. The long term reproducibility for lased zircon is  $\pm 0.1\text{‰}$ . At least four aliquots of Gore Mountain Garnet standard (UWG-2) were analyzed with each set of unknown analyses. The  $\delta^{18}\text{O}$  values for unknowns were corrected by 0.1–0.4‰ as determined by the difference of each day's UWG-2 value and 5.8‰, the accepted value of UWG-2 (Valley et al., 1995). For more than 90% of the samples in this study duplicate analyses were performed from the same zircon concentrate. These were generally analyzed on different days to further evaluate reproducibility of oxygen isotope ratios. In about 40% of these duplicate analyses (only in some samples of the CA2 and AL plutons) the zircon concentrate was separated to several size fractions to test for a possible correlation of size and  $\delta^{18}\text{O}$  value, which could suggest inheritance or zoning. Duplicate analyses of the same zircon concentrate (either undivided or of different size fractions) show a very restricted range:  $\pm 0.00\text{--}0.04\text{‰}$  (Appendix A) of the average  $\delta^{18}\text{O}$  (Zrn) value, manifesting the excellent ( $<0.1\text{‰}$ ,  $1\sigma$  external error, see above) reproducibility of the analyses of this study. In cases tested, size was shown to have no measurable effect on the  $\delta^{18}\text{O}$  value. Larger variability of the  $\delta^{18}\text{O}$ (Zrn) value is reported for several rock units (up to 0.39‰; Table 2). This variability stems from averaging  $\delta^{18}\text{O}$ (Zrn) values of zircon aliquots extracted from different samples (represent-

ing different geographical locations or chemistries) of the same rock unit.

## 5. Results

### 5.1. Homogeneity of $\delta^{18}\text{O}$ (Zrn) in analyzed rocks

$\delta^{18}\text{O}$ (Zrn) values of all studied rocks vary from 4.5 to 8.2‰ (Tables 1, 2). For more than 80% of the rocks, two or more samples representing the geographical or compositional variability within the rock unit were analyzed. In these cases, variability within one pluton, dyke or sub-volcanic body is restricted to  $\pm 0.01$  to  $\pm 0.39\text{‰}$  ( $1\sigma$ ), of the average  $\delta^{18}\text{O}$  (Zrn). However, the average variability for a multiply sampled rock is much lower: only  $\pm 0.15\text{‰}$  ( $1\sigma$ ) of the average of  $\delta^{18}\text{O}$ (Zrn) value, manifesting the homogeneity of most igneous bodies and the preservation of magmatic isotope ratios in the zircons. Except for two plutons (i.e., Zreir and Hibran-Miar, Table 2), all investigated rocks with  $\delta^{18}\text{O}$ (Zrn) variability between  $\pm 0.15\text{‰}$  and  $\pm 0.39\text{‰}$ , yielded mildly-elevated to high- $\delta^{18}\text{O}$ (Zrn) values of 6.1 to 8.2‰. In cases of higher than mantle-like  $\delta^{18}\text{O}$ (Zrn), such sample variability can be interpreted to represent different degrees of interaction with supra-crustal material within the ascending magma. The Hibran-Miar and Zreir plutons however, show a mantle-like average  $\delta^{18}\text{O}$ (Zrn) but  $\pm 0.24\text{‰}$  and  $\pm 0.39\text{‰}$  sample variability [of the average  $\delta^{18}\text{O}$ (Zrn)], respectively. It is important to note that although variable within 0.2 to 0.4‰, all samples of these plutons yielded  $\delta^{18}\text{O}$ (Zrn) values that are within the mantle-like  $\delta^{18}\text{O}$  range of  $5.3 \pm 0.6\text{‰}$  for zircon (Appendix A). The large compositional range and the zoned character of these plutons ( $\text{SiO}_2$ : ~50–72 wt.%; quartz-diorites to monzogranites) implies a complex structure with multiple intrusions. While the variable  $\delta^{18}\text{O}$  (Zrn) values for individual samples in the Hibran-Miar or Zreir plutons could be explained by derivation from different sources the latter are dominantly mantle-like in terms of  $\delta^{18}\text{O}$ .

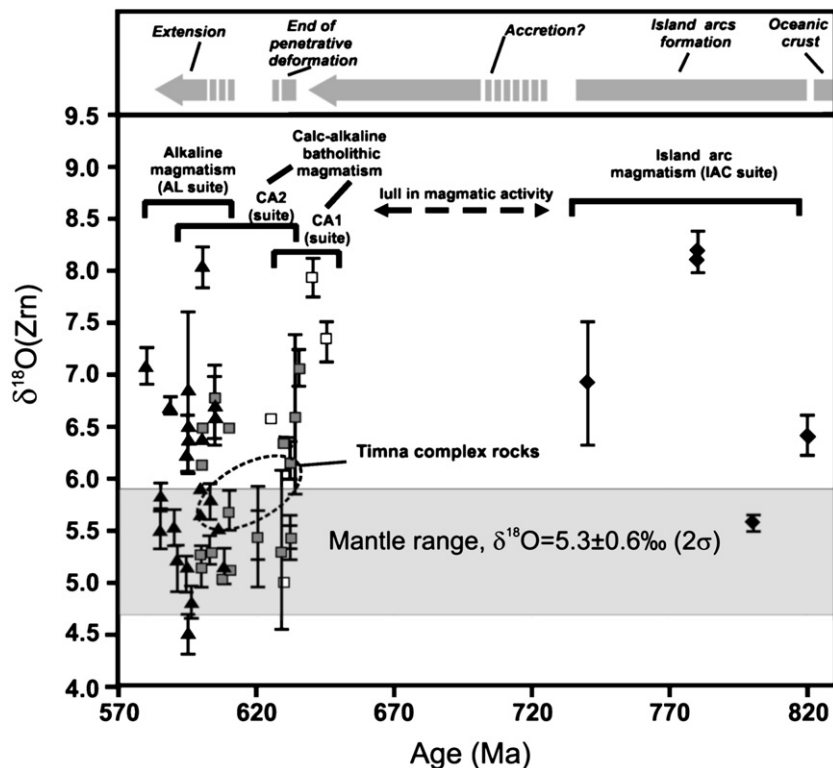


Fig. 5.  $\delta^{18}\text{O}$ (Zrn) vs. age for IAC, CA1, CA2 and AL sampled in this study. Arrows in the top section designate the development of the ANS lithosphere in this region. For details see text.

## 5.2. Oxygen isotope ratios of pre- to syn collisional rocks

The pre- to syn-collisional tectono-magmatic settings (i.e., IACs and CA1 suites) are represented here mainly by  $\delta^{18}\text{O}(\text{Zrn})$  of schists, gneisses and deformed plutons. The IAC samples (820–740 Ma) include the Elat-schist and several gneiss samples from the Elat-IAC in the northeast and one gneiss sample (Aliat gneiss) from the Feiran-IAC in the northwest (Fig. 1). The oldest zircons sampled here are the detrital zircons of the Elat-schist (870–780 Ma, but mostly 820 Ma) at  $\delta^{18}\text{O}=6.4\%$  and igneous zircons of the Aliat gneiss (~800 Ma) at  $\delta^{18}\text{O}=5.6\%$  from the Elat- and Feiran-IACs, respectively (Table 2). Zircons from three other gneisses of the Elat-IAC spanning an age of 780–740 Ma yielded  $\delta^{18}\text{O}(\text{Zrn})$  values of 6.9 to 8.2% (Table 2).

The CA1 (650–630 Ma) samples include deformed plutons from southern Israel and from the Kid area (Figs. 1 and 2). Deformed plutons of this phase from southern Israel (i.e., Shahmon metagabbro/diorite, Shahmon granitic gneiss, Table 2) yielded  $\delta^{18}\text{O}(\text{Zrn})$  values of 7.3% to 7.9%, while those sampled in the Kid area (Rurabi and Jantil deformed plutons, Table 2) yielded  $\delta^{18}\text{O}(\text{Zrn})$  values of 5.0 to 6.6%.

Using the  $\delta^{18}\text{O}(\text{Zrn})$  data, the average  $\text{SiO}_2$  contents, and eqn. 1 for  $\Delta(\text{WR-Zrn})$  from Valley et al. (2005) results in a  $\delta^{18}\text{O}(\text{WR})$  range of 6.2 to 10.0% for the magma precursors of the gneisses and deformed granitoids of the IAC+CA1 suites (Table 2).

## 5.3. Oxygen isotope ratios of CA2 and AL rocks

Post-collisional batholithic calc-alkaline (CA2) and alkaline to peralkaline (AL) rocks comprise the main sample sets of this study (CA2:  $n=18$  rocks, AL:  $n=23$  rocks; Table 2). The  $\delta^{18}\text{O}(\text{Zrn})$  of CA2 and AL are presented in Fig. 5 alongside  $\delta^{18}\text{O}(\text{Zrn})$  from the older rock suites. The  $\delta^{18}\text{O}(\text{Zrn})$  values of the CA2 suite rocks range from 5.1 to 7.1% [(5.8±0.7%, 1 $\sigma$ ), Fig. 6a, Table 2]. The AL suite rocks have a comparable average value [(6.0±0.8%, 1 $\sigma$ ), Table 2], but a wider range of  $\delta^{18}\text{O}(\text{Zrn})$  values: 4.5 to 8.0% (Fig. 6b, Table 2). Using the  $\delta^{18}\text{O}(\text{Zrn})$  data and eqn. 1 from Valley et al. (2005) results in  $\delta^{18}\text{O}(\text{WR})$  ranges of 6.3 to 9.2% and 6.3 to 10.1% for magmas of the CA2 and the AL suites respectively (Table 2). Since our sampling included many small-scale (~1–5 km<sup>2</sup>) intrusions and units of volcanic rocks in southern Israel, but much larger (up to ~200 km<sup>2</sup>; multiply sampled) intrusions and thicker volcanic sequences in Sinai (Table 2), the average  $\delta^{18}\text{O}(\text{Zrn})$  value of each suite may be biased by the over-representation of the southern Israel samples. Normalization using the surface exposure of each rock, a reasonable first approximation for its volume contribution to the average  $\delta^{18}\text{O}(\text{Zrn})$  value, was applied. The “volume normalization” yielded average  $\delta^{18}\text{O}(\text{Zrn})$  values of 5.7‰ and 5.8‰ [equivalent to  $\delta^{18}\text{O}(\text{WR})$  values of 7.4 and 7.7‰ using volume normalized  $\text{SiO}_2$  contents] for the CA2 and AL suites, respectively (Fig. 6a and b), showing that the two suites are indistinguishable by their average  $\delta^{18}\text{O}(\text{Zrn})$  values. Thus, both the post-collisional calc-alkaline (CA2) and alkaline (AL) magmatic suites are volumetrically dominated by rocks derived from mantle-like  $\delta^{18}\text{O}$  sources. Only a small proportion (volumetrically) of rocks from these suites have mildly higher  $\delta^{18}\text{O}(\text{Zrn})$  values (up to ~8.0‰, Tables 1, 2) and bear evidence for some contribution from supracrustal sources.

Being isotopically indistinguishable (i.e., “volume normalized” average  $\delta^{18}\text{O}(\text{Zrn})$  of CA2=5.7‰ and AL=5.8‰ Fig. 6a and b), the CA2 and AL suites were joined together to inspect the general spatial variation of  $\delta^{18}\text{O}(\text{Zrn})$  in Sinai and southern Israel (Fig. 1). In spite of the rather limited range of  $\delta^{18}\text{O}(\text{Zrn})$  values measured in the CA2 and AL rocks within the studied area (4.5 to 8.0‰; 90% are within 5 to 6.7‰, Tables 1, 2), geographical zoning is observed in the form of two regions of differing isotope ratios. Mantle-like  $\delta^{18}\text{O}(\text{Zrn})$  values characterize the majority of the studied area in southernmost Sinai (~8000 km<sup>2</sup>) but the northwestern belt is characterized by higher  $\delta^{18}\text{O}(\text{Zrn})$  values (Figs. 1 and 2) except for the Nastrin gabbro (40 km<sup>2</sup>) and a few minor (<2 km<sup>2</sup>) intrusions in Timna complex characterized by mantle-like

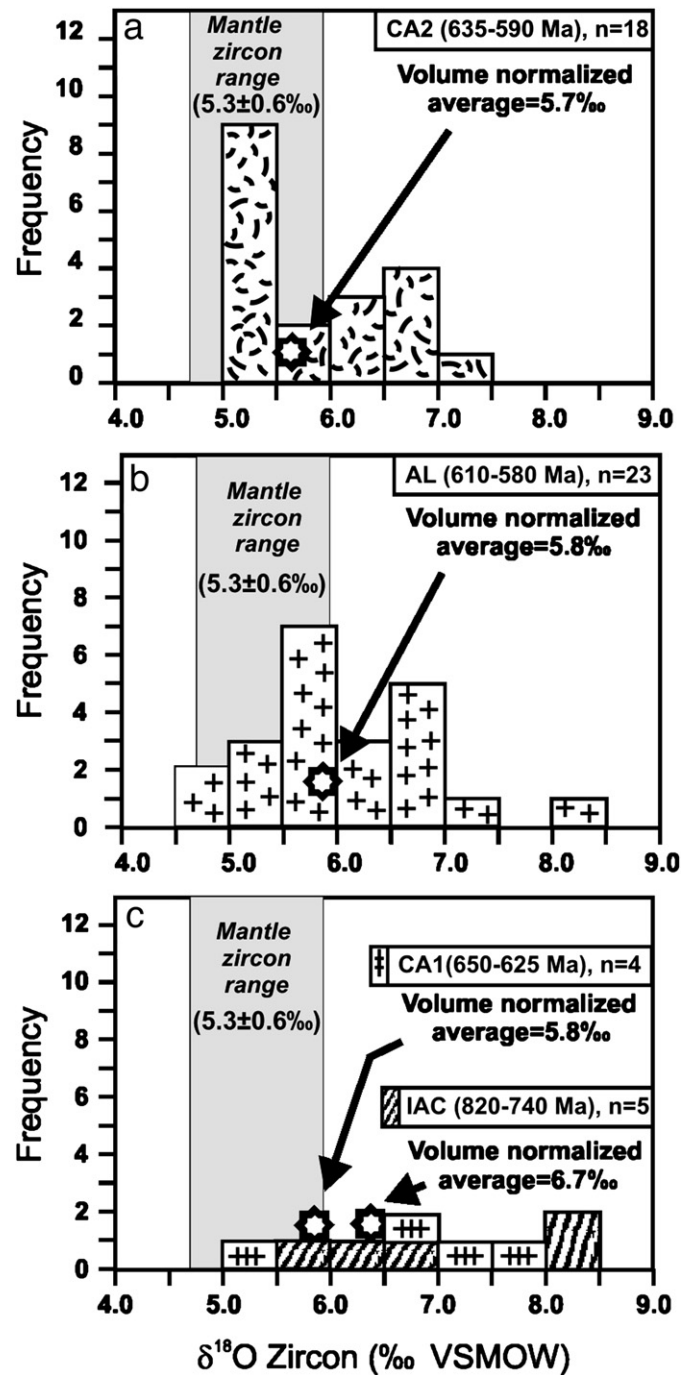


**Fig. 6.** Histograms of  $\delta^{18}\text{O}(\text{Zrn})$  for (a) CA2 rocks (635–590 Ma), (b) AL rocks (608–580 Ma), and (c) IAC and CA1 rocks (820 Ma to ~635–625 Ma). Volume normalized average  $\delta^{18}\text{O}(\text{Zrn})$  values are shown for all suites.

$\delta^{18}\text{O}(\text{Zrn})$  (Table 2). The two regions are divided by a SW–NE trending “6‰ line” in Fig. 1. In most of the studied area this “high- $\delta^{18}\text{O}$ ” region is bordered to the north by Phanerozoic sedimentary cover, limiting its exposure to a narrow (~20–50 km wide) SW–NE trending belt-like feature. Recalculation to WR values, the southern region is characterized by  $\delta^{18}\text{O}(\text{WR})$  values of 6.3 to 8.0% for 55–76 wt.%  $\text{SiO}_2$  magmas while the northwestern belt is mostly characterized by  $\delta^{18}\text{O}(\text{WR})$  values of 7.9 to 10.1% for 61–76 wt.%  $\text{SiO}_2$  magmas and a volume normalized  $\delta^{18}\text{O}(\text{WR})$  of 8.5%. The  $\delta^{18}\text{O}(\text{Zrn})$  variability across the 6‰ line is not accompanied by any evident trend in the chemical or structural features of CA2 and AL rocks, nor is there any change in the timing of CA2 and AL events across this border. Good examples for this observation are the two large ring complexes in Sinai (Iqna and

Katharina rocks, Table 2), which straddle the 6‰ line to the NW and SE respectively (Fig. 1). While the two complexes are coeval [injection ages of Iqna and Katharina granites are  $578 \pm 8$  and  $583 \pm 6$  respectively, Be'eri-Shlevin et al. (2009)] and share similar chemical and structural features, the Katharina ring complex rocks (SE-region) are characterized by mantle-like  $\delta^{18}\text{O}(\text{Zrn})$  while the Iqna ring complex rocks (NW-belt) are characterized by high- $\delta^{18}\text{O}(\text{Zrn})$  values (Table 2). Importantly,  $\delta^{18}\text{O}(\text{Zrn})$  values of somewhat older volcanics and the syenogranite which intrude them are consistent within each ring complex. This observation further implies that the  $\delta^{18}\text{O}(\text{Zrn})$  differences between rocks of the two ring complexes are associated with their different source regions rather than with different formation processes.

As detailed above, several outliers in the northwestern belt are characterized by mantle-like  $\delta^{18}\text{O}$  compositions. It may be of importance to note that (a) all these outliers ( $n=4$ ) are of the AL suite (b) half ( $n=2$ ) of these AL intrusions are mafic, and they are the only truly mafic representatives of this suite (c) the 3 small-scale AL outliers of the Timna complex are located in the northernmost ANS exposures of southern Israel (i.e., the northernmost ANS exposure in the study area; Figs. 1 and 2) and their  $\delta^{18}\text{O}$  composition stands in contrast to all other ( $n=10$ ) CA2 and AL rock units measured in southern Israel (i.e., characterized by mildly-elevated  $\delta^{18}\text{O}$  compositions).

## 6. Discussion

### 6.1. Crustal recycling during the early history of the ANS

Isotope evidence for recycling of crust at an early East African orogenic stage (820–740 Ma) is first given here by the higher than mantle bulk  $\delta^{18}\text{O}(\text{Zrn})$  value of 6.4‰ determined for detrital zircons from the Elat schist of the Elat-IAC (Figs. 1 and 5c, Tables 1, 2). While the ages of these zircons cluster around ~820 Ma, it has been shown that they range from ~870 Ma to ~780 Ma (Kolodner et al., 2006; Kolodner 2007; Be'eri-Shlevin unpublished U–Pb ion-microprobe dating). Thus previous interpretations of the pelitic-psammitic Elat schist as derived from a single, proximal volcanic arc (Bentor, 1985; Kröner et al., 1990; Eyal et al., 1991; Kolodner et al., 2006) are not consistent with the new geochronology. Regardless of being derived from a single or multiple sources, the Elat-schist is characterized by  $\epsilon\text{Nd}$  values of +3 to +5 and  $\text{Sr}_i$  values of  $0.7030 \pm 0.0006$ , and thus considered to represent an integral part of the juvenile ANS with no contamination by old crustal components (Halpern and Tristan, 1981; Bielski, 1982; Stein and Goldstein, 1996; Stern, 2002; Stein, 2003).

The ages of the detrital zircons span ~100 m.y. However, simple magmatic growth within their protoliths is indicated by the textural and geochemical characteristics of these grains as well as by the lack age zoning (Kolodner, 2007; Be'eri-Shlevin unpublished U–Pb ion-microprobe dating). Metamorphic overgrowths of considerable size which could affect the  $\delta^{18}\text{O}(\text{Zrn})$  value were not detected by CL imaging or ion-microprobe dating. The bulk  $\delta^{18}\text{O}(\text{Zrn})$  value of 6.4‰ is interpreted here to represent mixture of magmatic sources represented by the zircons supplied to the sedimentary protolith of the Elat-schist. While important information concerning each magmatic source that contributed zircons to the Elat schist is masked by the mixed value, simple calculations show that one end member of this mixture must be characterized by higher than the mantle-like  $\delta^{18}\text{O}(\text{Zrn})$  range of  $5.3\% \pm 0.6$  ( $2\sigma$ ). The importance of this finding is that at ~780 Ma (age of the youngest detrital zircon) a mature arc was already established and at least some of its magmas assimilated high- $\delta^{18}\text{O}$  components. Thus, crustal recycling is recorded within the oldest rocks of the northernmost ANS. Future investigations of the Elat schist detrital zircons using high-resolution ion-microprobe  $\delta^{18}\text{O}$  analysis correlated with other intra grain characteristics (age, trace element patterns; Cavosie et al., 2006) will further unveil the earliest tectono-magmatic evolution of the northern ANS. For the sake of simplicity we will refer in the following text to the age of the Elat schist as ~820 Ma

(e.g., Kolodner et al., 2006) and thus the age of IAC formation in the region will be referred to as ~820–740 Ma.

It is not surprising, though, that not all early magmas show elevated  $\delta^{18}\text{O}$  compositions. Our sample of the ~800 Ma Aliat paragneiss from the Feiran-IAC yielded a  $\delta^{18}\text{O}(\text{Zrn})$  value of 5.6‰ (Table 2). Similar hornblende-biotite banded gneisses of the Feiran-IAC were defined as paragneisses and interpreted to represent high-grade metamorphism of a sedimentary source (El-Shafei and Kusky, 2003 and references therein). The Aliat gneiss is peraluminous ( $A/\text{CNK}=1.5$ ) and thus fits the paragneiss definition however, ion-microprobe dating of zircons from this gneiss shows a single age population of ~800 Ma with no evidence of xenocrysts or metamorphic overgrowths (Be'eri-Shlevin, 2008). Moreover zircons from this sample are euhedral, not rounded (Fig. 4b). Thus, there is no evidence of a sedimentary source in the zircon characteristics. Given a sedimentary protolith for the Aliat gneiss, the age range and shape of zircons identify only one single proximal source for these sediments. Unlike the Elat-schist, the bulk  $\delta^{18}\text{O}(\text{Zrn})$  value of 5.6‰ of the Aliat paragneiss represents derivation from normal, mantle-like  $\delta^{18}\text{O}$  sources without evidence of supracrustal contribution.

Younger IAC-gneisses (780–740 Ma, Table 1) are all from southern Israel and show  $\delta^{18}\text{O}(\text{Zrn})$  values of 6.9–8.2‰ (Fig. 6c, Table 2), well above the mantle-like  $\delta^{18}\text{O}(\text{Zrn})$  range. A magmatic origin for these zircons with no evidence of metamorphic overgrowths is indicated by CL imaging (this work; Fig. 4c) and by ion-microprobe dating (Kolodner, 2007; Be'eri-Shlevin unpublished U–Pb ion-microprobe dating). The consistently high- $\delta^{18}\text{O}(\text{Zrn})$  values of the post Elat-schist, IAC orthogneisses, especially the >8‰ values of Taba and Roded orthogneisses (780 Ma, Table 2), which are intrusive into metasedimentary country rocks of Elat schist [ $\delta^{18}\text{O}(\text{Quartz})=13.4\%$ ; Appendix A], may suggest significant intra-crustal recycling by magma mixing or assimilation within the crust (Valley et al., 2005). Intrusion of these magmas into a hot metamorphic terrane (Matthews et al., 1989; Katz et al., 1998; Garfunkel, 1999) would promote assimilation at this stage. The range of  $\delta^{18}\text{O}(\text{Zrn})$  of early (820–740 Ma) magmas of the northern ANS in Sinai and southern Israel is summarized in Table 1 and Figs. 5 and 6c. The variability of  $\delta^{18}\text{O}(\text{Zrn})$  values is interpreted to represent intra-crustal recycling i.e., assimilation of buried sediments or other supracrustal material within the crust. Importantly, Fig. 6c also shows that some early magmas (Aliat paragneiss, Table 2) were not affected by such processes, and show a mantle-like  $\delta^{18}\text{O}(\text{Zrn})$  composition. The important observation here is that at ~740 Ma, the newly formed IAC crust of the northernmost ANS was partially characterized by high- $\delta^{18}\text{O}$  components.

### 6.2. Calc-alkaline magmatism during late terrane accretion (650–625 Ma)

The initiation of batholithic calc-alkaline magmatism (CA1 suite 650–625 Ma) is coeval with the final collision of terranes in this area (Katz et al., 2004; Be'eri-Shlevin et al., 2009). The deformed CA1 plutons yield  $\delta^{18}\text{O}(\text{Zrn})$  values ranging from 5.0 to 7.9‰ equivalent to  $\delta^{18}\text{O}(\text{WR})$  values of 6.2 to 10.0‰ ( $n=4$ ; Table 2). Zircons are oscillatory zoned (Fig. 4d and e) and show no evidence of metamorphic rims, thus the  $\delta^{18}\text{O}(\text{Zrn})$  values are interpreted as magmatic. Of the four CA1 rocks sampled, three yield higher than mantle-like  $\delta^{18}\text{O}(\text{Zrn})$  values (Fig. 6c). High- $\delta^{18}\text{O}$  CA1 magmas could form by assimilation of buried supracrustal components at mid-upper crustal levels, and thus recycling of supracrustal material continued at this stage.

### 6.3. Isotope constraints on magma sources of the CA2 and AL suites

The main data set of this study comprises the  $\delta^{18}\text{O}(\text{Zrn})$  of post-collisional rocks (CA2 suite: ~635–590 Ma and AL suite: ~608–580 Ma, respectively) from southern Israel and Sinai (Egypt). Both suites formed after the major accretion of terranes and subduction have already ceased. Simple magmatic formation of zircon is indicated by

the lack of metamorphic overgrowths and the scarcity of xenocrystic zircon (Fig. 4f–h).

Several important observations can be made from the new values of  $\delta^{18}\text{O}(\text{Zrn})$  values reported here for the CA2 and AL suites:

- (1) The average  $\delta^{18}\text{O}$  values of both suites [ $\delta^{18}\text{O}(\text{Zrn})$  of 5.7 and 5.8‰ for the CA2 and AL suites respectively] suggest that volumetrically, they are dominated by sources of mantle-like  $\delta^{18}\text{O}$  composition that had no interaction with supracrustal components. The  $\delta^{18}\text{O}(\text{Zrn})$  values of the ~820–640 Ma IAC and CA1 magmas measured in this study show that at least parts of the ANS crust were "enriched" by high- $\delta^{18}\text{O}$  components prior to CA2 and AL magmatism (Fig. 6c). This discrepancy is critical for discussing the petrogenesis of CA2 magmas since several authors have suggested they derive from melting of the previously formed crust (i.e., IAC+CA1 material; Beyth et al., 1994; Stein, 2003). Unless systematic vertical or regional variability in the  $\delta^{18}\text{O}$  of the older crust is considered, the 820–640 Ma crust is not a probable reservoir for the main volume of CA2 (635–590 Ma) and AL (~610–580 Ma) magmas.
- (2) Rocks of the CA2 and AL suites differ in geochemical characteristics, age ranges, fractionation paths and depths of intrusion (Bentor and Eyal, 1987; Beyth et al., 1994; Garfunkel, 1999; Stein, 2003; Jarrar et al., 2003; Be'eri-Shlevin et al., 2009). However, the two suites display similarities in terms of  $\text{Sr}$ ,  $\epsilon\text{Nd}(\text{T})$  and  $\epsilon\text{Hf}(\text{T})$  values (Stein and Goldstein, 1996; Moghazi et al., 1998; Stein, 2003; Jarrar et al., 2003; Morag et al., 2007). Such similarities led Jarrar et al. (2003) to recognize that it is difficult to call upon a different tectonic setting for each suite. Furthermore, Be'eri-Shlevin et al. (2009) showed that intrusions from the two suites were coeval over ~20 Ma. Comparison of  $\delta^{18}\text{O}(\text{Zrn})$  from CA2 and AL suites in this region shows that they are also indistinguishable in terms of the "volume-normalized" average  $\delta^{18}\text{O}$  values [CA2:  $\delta^{18}\text{O}(\text{Zrn})=5.7\text{‰}$ ,  $\delta^{18}\text{O}(\text{WR})=7.4\text{‰}$ ; AL:  $\delta^{18}\text{O}(\text{Zrn})=5.8\text{‰}$ ,  $\delta^{18}\text{O}(\text{WR})=7.7\text{‰}$ ] but have a somewhat different  $\delta^{18}\text{O}(\text{Zrn})$  ranges (CA2: 5.1 to 7.1‰; AL: 4.5 to 8.0‰; Fig. 6a and b, Table 1). Thus it seems that models inferring different tectonic settings and/or different magma sources must be re-evaluated with regard to the similarities in radiogenic and  $\delta^{18}\text{O}(\text{Zrn})$  values of the two suites and their coeval intrusion over 20 Ma.

- (3) Whereas CA2 and AL rocks have a similar oxygen isotope composition, grouping the two suites together reveals a systematic spatial distribution of  $\delta^{18}\text{O}(\text{Zrn})$ . The geographical zoning of  $\delta^{18}\text{O}$ , first discovered here, is highlighted by the 6‰ line in Fig. 1, and has important implications for the sources of CA2 and AL magmas. The mantle-like  $\delta^{18}\text{O}$  of rocks to the south of this line further stresses the dominance of sources unaffected by interaction with surface processes in a large portion of the northern ANS. Nevertheless, the mildly elevated  $\delta^{18}\text{O}$  compositions of the NW-belt of intrusions [where mostly  $\delta^{18}\text{O}(\text{Zrn})=6.1\text{--}7.1\text{‰}$  equivalent to  $\delta^{18}\text{O}(\text{WR})=7.9\text{--}9.4\text{‰}$ ; and only one intrusion displays higher values of  $\delta^{18}\text{O}(\text{Zrn})=8.0\text{‰}$ ; Table 2] calls for a significant supracrustal contribution in this belt. We also note that within the restricted mantle-like  $\delta^{18}\text{O}(\text{Zrn})$  range of 4.5 to 5.9‰ of the southern area, values increase to the northwest approaching the 6‰ line (Figs. 1 and 7) thus the transition between the two terranes is gradual.
- (4) Based on the temporal and spatial association of mafic and felsic alkaline intrusions and on trace element patterns, the AL magmas were interpreted to derive from the lithospheric mantle and silicic rocks were typified as A-type granites (Beyth et al., 1994; Kessel et al., 1998; Mushkin et al., 1999, 2003; Stein, 2003; Jarrar et al., 2003; Katzir et al., 2007b; Jarrar et al., 2008). Mushkin et al. (1999, 2003) suggested that such alkali granite magmas were derived from parental mafic magmas of the lithospheric mantle by extensive fractionation (>90%). Whereas this model can explain the origin of most AL magmas, the  $\delta^{18}\text{O}(\text{Zrn})$  data presented here suggest a more complex scenario for sources of AL magmatism in the northernmost ANS. The dominance of mantle-like  $\delta^{18}\text{O}(\text{Zrn})$  values for AL rocks expressed by the volume normalized average of 5.8‰ is consistent with mantle derived parental melt with no crustal assimilation. The occurrence of mafic AL intrusions with mantle-like  $\delta^{18}\text{O}$  compositions, as outliers in the high- $\delta^{18}\text{O}$  northwestern belt is also consistent with this model. However, the existence of mildly-elevated  $\delta^{18}\text{O}(\text{Zrn})$  AL rocks within the northwestern belt is in apparent contrast to this model. Our results point to a bimodal population of AL magmas characterized by mantle-like  $\delta^{18}\text{O}$  vs. high- $\delta^{18}\text{O}$  compositions in the two regions described above (Fig. 1). Such variation in the  $\delta^{18}\text{O}$

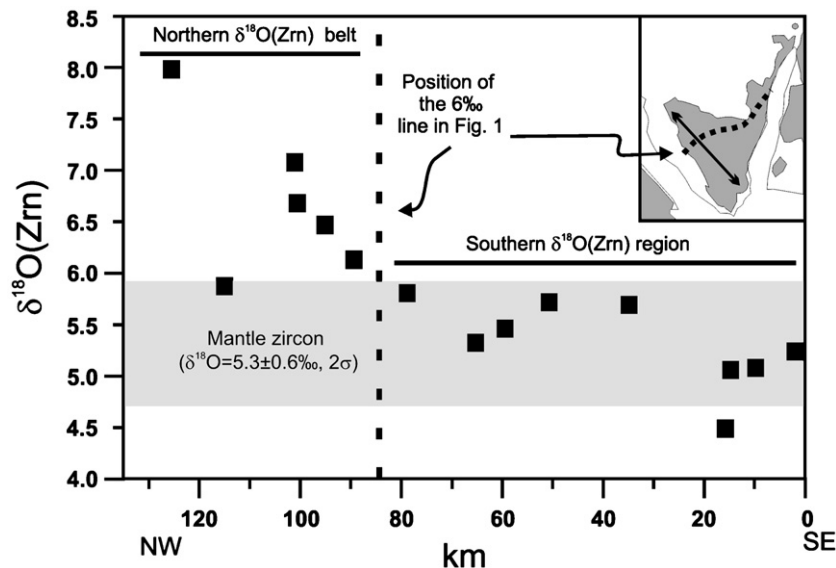


**Fig. 7.** Variation of  $\delta^{18}\text{O}(\text{Zrn})$  in rocks of the CA2 and AL suites (grouped together here) along a SE to NW section positioned at right angle with the 6‰ line of Fig. 1. The approximate position of this traverse is shown in the inset. Within the restricted mantle-like  $\delta^{18}\text{O}(\text{Zrn})$  range of 4.5–5.9‰ of the southern area, values increase to the northwest approaching the 6‰ line and beyond it indicating to the gradual transition between the two regions.

composition of ANS AL magmas was previously recognized by Katzir et al. (2007b), but their spatial distribution was not determined. In light of the long standing controversy as to the A-type granite petrogenesis (see Bonin, 2007 for a review) it is clearly shown here that in the northernmost ANS, formation of some A-type granites involved assimilation of crustal material.

#### 6.4. Quantifying supracrustal input to CA2 and AL magmas

In order to reconcile the different observations discussed above, identification of possible reservoirs and quantifying their involvement in the generation of CA2 and AL magmas must first be attained. While  $\delta^{18}\text{O}$  (Zrn) is used here as a tracer for supracrustal input into magma sources it is important to note that this tracer does not distinguish between possibly mafic lower crust and the lithospheric mantle if both had no interaction with supracrustal material. Our calculations use eqn. 1 (Valley et al., 2005), and the average  $\text{SiO}_2$  wt.% for rocks (Table 2).

Evidence for the  $\delta^{18}\text{O}$  composition of the crust prior to initiation of CA2 and AL magmatism comes from the  $\delta^{18}\text{O}$ (Zrn) values of several IAC and CA1 rocks. These indicate that at least some parts of the crust were enriched by high- $\delta^{18}\text{O}$  components prior to ~635 Ma, but do not preclude vertical or regional  $\delta^{18}\text{O}$  variability within this crust. During subduction related magmatism, assimilation of high- $\delta^{18}\text{O}$  components could have taken place at intermediate levels of the crust while mantle derived mafic melts accumulated below forming a purely mantle-like  $\delta^{18}\text{O}$  lower crust. Regional variation in the  $\delta^{18}\text{O}$  composition of the pre-635 Ma crust may have also existed. Since all IAC samples studied here come from the northwestern high- $\delta^{18}\text{O}$  belt (Fig. 1) they may not represent the pre-635 Ma crust of the equivalent crust to the southeast.

The mantle-like  $\delta^{18}\text{O}$ (Zrn) values of CA2 and AL magmas in the southeastern region imply that they could either evolved from mantle melts or formed by partial melting of mantle derived mafic lower-crust. The mildly-elevated  $\delta^{18}\text{O}$ (Zrn) values of CA2 and AL magmas [ $\delta^{18}\text{O}$ (WR)≈8.5‰] from the northwestern high- $\delta^{18}\text{O}$  belt suggest they formed with a contribution of a high- $\delta^{18}\text{O}$  component. However, even if metasediments are ruled out as potential contributors, partial melting of the pre-635 Ma, high- $\delta^{18}\text{O}$ , IAC+CA1 crust [high- $\delta^{18}\text{O}$  gneisses of  $\delta^{18}\text{O}$ (WR)≈9.3‰] alone would produce magmas with much higher  $\delta^{18}\text{O}$  values than those measured in the post-collisional suites. Mixing of a basaltic magma derived from mantle-like  $\delta^{18}\text{O}$  sources with melts derived from the high- $\delta^{18}\text{O}$  pre-635 Ma crust is a more probable mechanism for generating the mildly-elevated  $\delta^{18}\text{O}$  CA2 and AL magmas. In the following calculations, a basaltic magma [ $\text{SiO}_2=50$  wt.%;  $\delta^{18}\text{O}$ (WR)=5.9‰] is used to proxy the mantle-like source. An unaltered gneissic crust [ $\text{SiO}_2=65$  wt.%;  $\delta^{18}\text{O}$ (WR)≈9.3‰] which approximately represents a volume normalized average composition of the IAC+CA1 upper crust in the north (Table 2) is used as a minimum estimate for high- $\delta^{18}\text{O}$  contaminant.

Material balance calculation reveals that a minimum input of 30 to 70% of the high  $\delta^{18}\text{O}$  contaminant into mantle-like  $\delta^{18}\text{O}$  parent magmas is required to reproduce the  $\delta^{18}\text{O}$ (Zrn) range of 6.1 to 7.1‰ which characterizes all but one of CA2 AL rocks this region (Table 2). A more reasonable estimate for the pre-635 Ma crust would also include metasediments and altered gneisses that would raise the  $\delta^{18}\text{O}$ (WR) value of the crust to 12 to 15‰. This agrees with the measured  $\delta^{18}\text{O}$ (Qtz)=13.4‰ in Elat schist (Appendix A). Using the higher  $\delta^{18}\text{O}$  crustal estimate, a reasonable input of ~15 to 35% contaminant crust into the mantle-like  $\delta^{18}\text{O}$  basalt reproduces the expected  $\delta^{18}\text{O}$ (Zrn) values of CA2 and AL rocks.

#### 6.5. A tectono-magmatic model for the generation of CA2 and AL magmas

Several features constrain the sources and petrogenesis of CA2 and AL magmas in the northernmost ANS. The two suites display different geochemical features and slightly different intrusion time spans, but also similarities in the isotope (Sr, Hf, Nd, O) composition and an

overlap of ~20 m.y. The  $\delta^{18}\text{O}$ (Zrn) provinciality also bears important implications for their genesis. Here we aim to explain these different features via a tectono-magmatic model.

The identity of the sources that generated the voluminous, mostly granitic, post-collisional calc-alkaline suite (CA2) are debated (Stein, 2003). Some authors suggested that these magmas were generated by anatexis of the older, IAC, crust (Beyth et al., 1994; Moghazi et al., 1998; Stein, 2003). In contrast, Jarrar et al. (2003) favored subducted oceanic crust as their source, but noted that there is no evidence for ongoing subduction in this region at the time of intrusion of the CA2 suite (Katz et al., 2004). Possible sources for CA2 magmas include the asthenospheric/lithospheric mantle and the mafic lower-crust. We favor the mafic lower-crust as a potential source because: (a) it is compatible with the major and trace element composition of the CA2 magmas (Beyth et al., 1994; Jarrar et al., 2003; Stein, 2003); (b) such crust could have been formed during the earlier history of the ANS without necessarily incorporating high- $\delta^{18}\text{O}$  components, thus satisfying the conditions for mantle-like  $\delta^{18}\text{O}$  CA2 magmas; (c) genesis of CA2 magmas from the mantle requires unreasonable amount of melts in the asthenospheric/lithospheric mantle (>60% of the exposed crust in Sinai is granitic-granodioritic); and (d) fractionation of such melts would also require formation of very large amounts of residual material not yet recognized in the ANS. The formation of AL magmas was partially coeval with late stages of CA2 magmatism, but several features including its bimodal (mafic-felsic) character; the intrusion into shallow levels of the crust and its alkaline chemistry can be more easily explained via melting of the lithospheric mantle (Beyth et al., 1994; Mushkin et al., 2003; Jarrar et al., 2003). Since CA2 and AL magmas of the northwestern belt show only mildly-elevated  $\delta^{18}\text{O}$  compositions, derivation solely from melting of the IAC+CA1 crust of this region is unlikely and a mantle-like  $\delta^{18}\text{O}$  end member is required. We suggest that sources of most CA2 and AL magmas of the northernmost ANS were characterized by mantle-like  $\delta^{18}\text{O}$  compositions, but that incorporation of ~15 to 35% IAC+CA1 high- $\delta^{18}\text{O}$  crust occurred at higher levels within the northwestern high- $\delta^{18}\text{O}$  belt. In this model, the CA2+AL  $\delta^{18}\text{O}$ (Zrn) provinciality simply represents variable extent of interaction between lower-crust/mantle derived magmas with the pre-635 Ma (intermediate-felsic) crust at mid crustal levels. Differences in crustal thickness between the two regions at ~635 Ma may account for such variability. A thicker crustal section at the northwestern belt could have promoted much larger extent of interaction between primitive parent magmas and the felsic crust.

Thicker crust in the northwestern belt, compared to the southeastern region, could have formed prior to CA2 and AL magmatism (>635 Ma) via higher rates of formation and accretion of island arcs. The occurrence of three IAC relicts (Feiran, Sa'al and Elat; Fig. 1) within the northwestern high- $\delta^{18}\text{O}$  belt may support such a reconstruction. The suggested thickened crust in a NE–SW trending belt also parallels some of the main sutures defined in more southern segments of the ANS (Stoeser and Camp, 1985; Stern, 1994; Abdelsalam and Stern, 1996; Fig. 1 inset). However, the palaeogeography of the early (pre 635 Ma) northernmost ANS and the character of each island arc terrane is yet poorly resolved (Bentor, 1985). Several features imply a single terrane rather than the amalgamation of allochthonous terranes prior to ~635 Ma: (a) the lack of ophiolite sutures hampers the identification of supposed different terranes (Bentor, 1985); (b) the growing evidence for ~820–740 Ma ages in all IAC relicts including the Kid IAC in the south (Blasband et al., 1997; Be'eri-Shlevin et al., 2009) are more consistent with IACs in the north and south forming at the same time and thus belonging to a single terrane; (c) The gradual transition in  $\delta^{18}\text{O}$ (Zrn) between the southeastern and northwestern regions (Fig. 7) suggests changes within a single terrane rather than a stepwise change expected from the amalgamation of two or more allochthonous terranes.

In contrast to models inferring formation of variable crustal thickness prior to ~635 Ma, models inferring extension during ~630–580 Ma can explain more easily many of the features discussed

above. Stern (1985) recognized that the Najd fault system can be detected across the Red Sea in Arabia and central Eastern Desert of Egypt, but could not be traced in the northernmost ANS including the northern Eastern Desert of Egypt, Sinai, Israel, and SW Jordan. In contrast, this region is characterized by vast intrusion of undeformed granitoids and show evidence of extension at about ~600 Ma. The model put forward by Stern (1985) implies a very strong relationship

between the development of the Najd fault system and fan-shaped rifting in the northernmost ANS. While problems associated with the structure of the Najd system are beyond the scope of this work, we note that the geometry of the fan shaped rifting within the northernmost ANS as suggested by Stern (1985) is concordant with many of our observations. Importantly, it can also explain how the variable NW–SE crustal thicknesses were formed at this time, thus

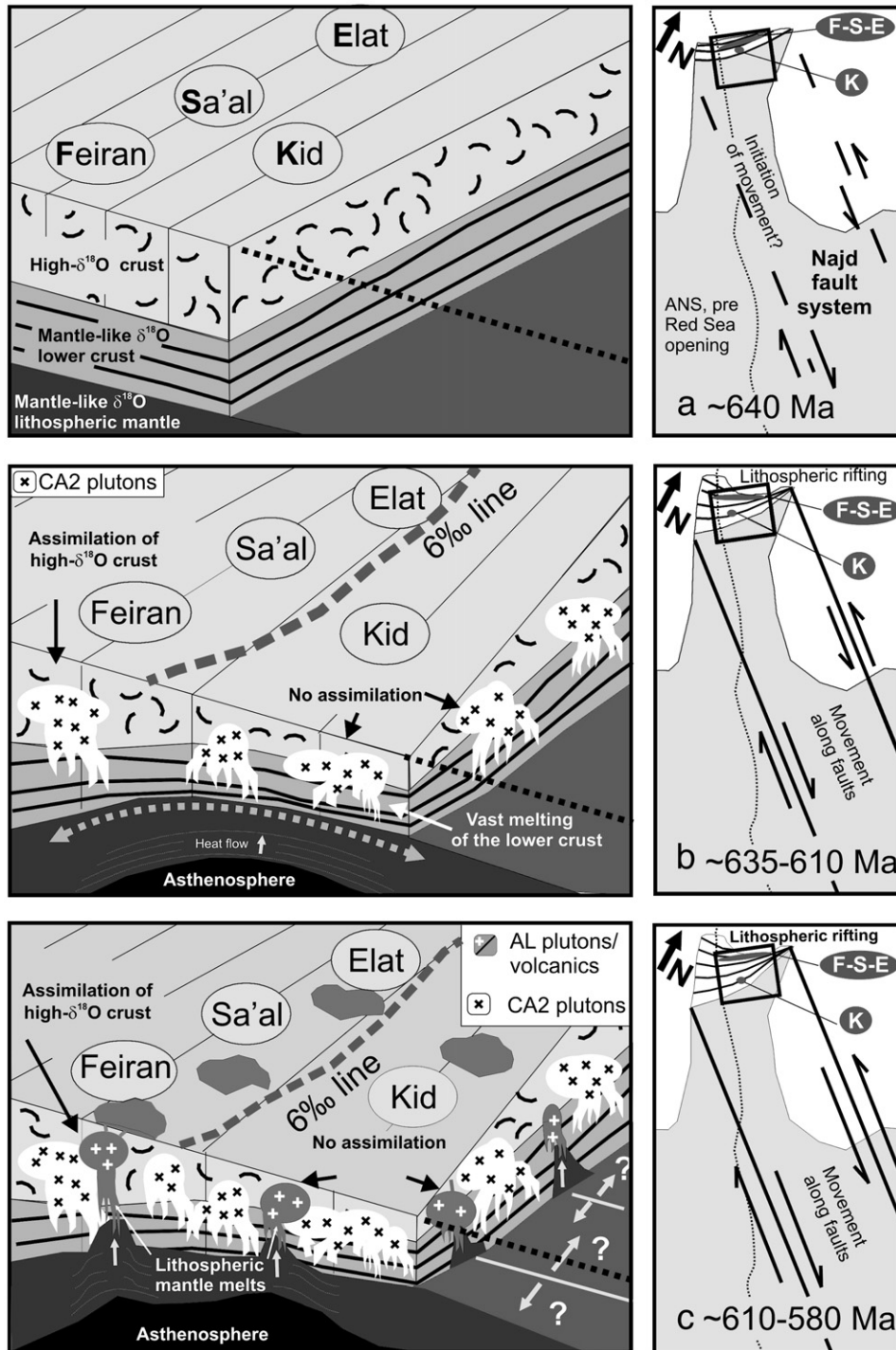


**Fig. 8.** A sketch model (not to scale) showing the proposed evolution of the northernmost ANS crust during rifting associated with strike slip movement along the Najd fault system (modified from Stern, 1985). Left column shows a lithospheric scale cross sections and the right column shows the associated map views. (a) Prior to extension (~640 Ma) the stratified crust included a high- $\delta^{18}\text{O}$  upper part but a mafic lower-crust of mantle-like  $\delta^{18}\text{O}$  composition. Fan shaped lithospheric rifting (b+c) produced variable crustal thicknesses where the southeastern region is much thinner than the northwestern region. Intrusion of CA2 and AL mantle-like  $\delta^{18}\text{O}$  parent magmas into the southeastern thinned crust did not involve much pre-635 Ma felsic crust assimilation. In contrast, the thicker crustal section in the northwestern belt promoted assimilation of such crust, introducing mild amounts of high- $\delta^{18}\text{O}$  material into these magmas. The 6‰ line is thus interpreted to approximate the NW–SE transition in crustal thickness during this time. F-S-E: Feiran-Sa'al-Elat IACs, K: Kid IAC.

impacting on the assimilation patterns of CA2 and AL parent magmas in the NW vs. the SE regions. The sketch model in Fig. 8 shows the proposed evolution of the northernmost ANS crust from ~635 Ma when CA2 magmatism commenced and up to 580 Ma when the last major episode of AL magmatism was over. The main assumption for the initial stage (~640 Ma) is that this crust was stratified in terms of  $\delta^{18}\text{O}$  composition with high- $\delta^{18}\text{O}$  upper parts formed during IAC and CA1 magmatism and an associated mafic lower-crust of mantle-like  $\delta^{18}\text{O}$  (Fig. 8a). Fan shaped rifting resulted in thinning of the northernmost ANS lithosphere excluding a NW region now exposed as a NE–SW trending belt (Fig. 8). Extension-assisted upwelling of the asthenospheric-mantle resulted in high heat flow that at ~635 Ma induced vast anatexis of the mafic lower-crust to form CA2 magmas (Fig. 8b). Later on (~610 Ma) percolation of mantle melts into this crust, possibly along Najd associated deep seated lithospheric scale faults, introduced AL magmas to shallow levels of the crust (Fig. 8c). Between ~610 and 590 Ma both CA2 and AL magmas were formed at different levels within the lithosphere (Be'eri-Shlevin et al., 2009). Intrusion of both CA2 and AL magmas in the southeast where the lithosphere was thin did not involve much felsic crust (IAC+CA1) assimilation. In contrast the thicker crustal section in the north-western belt promoted assimilation of such crust introducing mild amounts of high- $\delta^{18}\text{O}$  material into these magmas. The application of Stern's (1985) model to explain post-collisional magmatism in the northernmost ANS requires that rifting of the lithosphere commenced at 640–630 Ma. This estimate is ~30–40 m.y older than the timing of extension as deduced by field evidence including widespread injection of dykes and the formation of intra-montane basins (Beyth et al., 1994; Stern 1994; Garfunkel, 1999; Jarrar et al., 2003), but is remarkably similar to estimates of Stacey and Agar (1985) for the initiation of strike-slip movements along the Najd fault system. The discrepancy between the ~630 Ma and ~600 Ma estimates for extension in the northernmost ANS is easily resolved since lithospheric rifting commenced at deep levels and was associated with vast amounts of granitoid intrusions emplaced passively. Thus we do not expect to find surface manifestations of such rifting at this stage. Later on (<610 Ma), continued rifting was associated with shallow expressions of extension including the formation of molasse-volcanic filled basins, injection of large amount of dike swarms and emplacement of high levels intrusions. This change may also relate to the mostly brittle activity along the Najd fault system at this stage (Stern, 1985; Abdelsalam and Stern, 1996).

#### 6.6. Oxygen isotope provinciality in the ANS and Peninsular range batholith

Comparison of the  $\delta^{18}\text{O}$  provinciality of the CA2 and AL rocks revealed in this study with similar trends described by Taylor (1986) for the rocks of the Peninsular ranges batholith (PRB) in Baja California, shows that the two regions define very different tectonic scenarios. While the 600 km long  $\delta^{18}\text{O}(\text{WR})=8.5\%$  border between the eastern and western zones of the PRB is comparable with the  $\delta^{18}\text{O}(\text{Zrn})=6\%$  line in the northernmost ANS [equivalent to  $\sim\delta^{18}\text{O}(\text{WR})=8.5\%$ ], there are several features that clearly vary in the two regions: (a) The eastern and western regions of the PRB are distinct both in age and in composition including trace element patterns. In contrast, the CA2 and AL suites of Sinai and southern Israel do not show any evident trend in chemistry, timing of intrusion or structural pattern across the 6‰ line (Bentor and Eyal, 1987; Be'eri-Shlevin et al., 2009); (b) while the PRB is considered to have evolved during active subduction, the CA2 and AL magmas formed after subduction and collision had ceased in this region. Taylor (1986) suggested that underplating of the altered upper part of an oceanic slab beneath the eastern zone could explain the higher  $\delta^{18}\text{O}(\text{WR})$  of 9–11% of this part of the PRB. This model may be applicable to an active continental margin like the Tertiary PRB, but it cannot be applied to the northernmost ANS CA2 and AL magmas. Thus

$\delta^{18}\text{O}$  provinciality within the crust can develop via variable mechanisms and tectonic settings as displayed by the PRB and the CA2 and AL rocks of the northernmost ANS.

#### 6.7. An additional Neoproterozoic terrane to the north?

The northernmost samples in this study, the plutonic rocks of the Timna complex, located at the northern part of Neoproterozoic basement exposures in southern Israel (Figs. 1 and 2) yielded comparably lower  $\delta^{18}\text{O}(\text{Zrn})$  relative to the other, more southerly plutons in southern Israel (Fig. 7, Table 2). Whereas most CA2 and AL rocks of the southern Israel are assigned to the high- $\delta^{18}\text{O}$  belt, the Timna complex rocks may represent yet an additional discontinuity with a northern basement terrane poorly known due to cover by Phanerozoic sediments (Figs. 1 and 2).

### 7. Conclusions

1. Crustal recycling during the very early evolutionary stages of the northernmost ANS (820–740 Ma) is inferred from higher than mantle values of  $\delta^{18}\text{O}$  of several orthogneisses [ $\delta^{18}\text{O}(\text{Zrn})=6.9\text{--}8.2\%$ ; average  $\delta^{18}\text{O}(\text{WR})\approx 9.4\%$ ] and from the average  $\delta^{18}\text{O}(\text{Zrn})$  value of 6.4‰ determined for detrital zircons (~870–780 Ma) from the Elat-schist. The latter represent the oldest known source rocks in the region. Another gneiss of ~800 Ma has mantle-like  $\delta^{18}\text{O}(\text{Zrn})$  values of 5.6‰ implying that not all magmas involved crustal contributions.
2. The main sample set analyzed in this work comprises rocks of the post-collisional calc-alkaline (CA2: 635–590 Ma) and alkaline (AL: 608–590 Ma) suites. Felsic rocks of the AL suite display typical A-type granite characteristics. Rocks of the two suites are indistinguishable by their average  $\delta^{18}\text{O}(\text{Zrn})$  values of 5.7 to 5.8‰, which are within the mantle-like zircon range. Thus, melts derived solely from the intermediate-felsic pre-635 Ma crust that included high- $\delta^{18}\text{O}$  components cannot account for their formation and their sources should be sought in the mantle or in a mantle-like  $\delta^{18}\text{O}$  reservoir that resided within the lower crust.
3. In order to reconcile their different geochemical compositions and petrogenetic evolution, but similar dominant mantle-like  $\delta^{18}\text{O}$  compositions we suggest that CA2 magmas were derived from the mafic lower-crust, which was not contaminated by high- $\delta^{18}\text{O}$  components whereas AL magmas evolved from lithospheric-mantle melts.
4. Notwithstanding the dominance of mantle-like  $\delta^{18}\text{O}(\text{Zrn})$  compositions of the two suites, grouping them reveals a  $\delta^{18}\text{O}(\text{Zrn})$  geographic zoning and a “6‰ line” that separates a large southeastern region of  $\delta^{18}\text{O}(\text{Zrn})=4.5\text{--}5.9\%$  [ $\delta^{18}\text{O}(\text{WR})=6.9\text{--}8.2\%$ ] from a northwestern belt with  $\delta^{18}\text{O}(\text{Zrn})=6.1\text{--}8.0\%$  [ $\delta^{18}\text{O}(\text{WR})=7.9\text{--}10.1\%$ ]. Material balance calculations imply that parent magmas of both CA2 and AL magmas of the northwestern belt were derived from mantle-like  $\delta^{18}\text{O}$  reservoirs but assimilated 15–35% pre-635 Ma crust. In the southeastern region no assimilation of high- $\delta^{18}\text{O}$  material by CA2 and AL magmas occurred.
5. Our results show that some A-type granites of the northernmost ANS assimilated supracrustal material. This stands in contrast to previous views that interpreted them to be highly fractionated mantle melts with no crustal component.
6. The  $\delta^{18}\text{O}$  provinciality defined for the CA2+AL rocks may be explained if magmas derived from mantle-like  $\delta^{18}\text{O}$  sources intruded crustal terranes of different thicknesses. In accordance to the model proposed by Stern (1985) we suggest that fan shaped rifting of the northernmost ANS during the late Neoproterozoic resulted in a thicker crustal section in the northwestern belt and a thinner crust in the larger southeastern region. At ~635 Ma deep parts of the lithosphere began rifting, allowing the asthenospheric mantle to rise and heat the lithosphere. This resulted in vast melting of the mafic lower-crust to produce the batholithic CA2 suite magmas. Later

(~610 Ma) percolation of mantle melts (probably along deep seated lithospheric scale faults) introduced AL magmas to shallow levels of the crust. Intrusion of CA2 and AL magmas into the thinned southeastern crust did not involve assimilation of older crust whereas similar intrusion into the thicker northwestern crust resulted in mild assimilation of high- $\delta^{18}\text{O}$  pre-635 Ma crust.

## Acknowledgments

We thank Prof. M. Eyal and A. Gal-Steinitz for providing rock samples. G. Tirosch and E. Hasid are thanked for their help in mineral separation. M. Spicuzza is thanked for his assistance with the isotopic analytical work. Discussions with Prof. B. Litvinovsky and Dr. Ada Zanzilevich and reviews of two anonymous reviewers greatly improved the manuscript. This research was financially supported by the Israeli Science Foundation (ISF 142/02) grant, and by the Israel Ministry of Science and Technology grant 3-3571 for collaboration with Russia.

## Appendix A. Supplementary data

Supplementary data associated with this article can be found, in the online version, at doi:10.1016/j.lithos.2008.10.001.

## References

- Abdelsalam, M.G., Stern, R.J., 1996. Sutures and shear zones in the Arabian-Nubian Shield. *Journal of African Earth Sciences* 23, 289–310.
- Andersen, A., Abu El-Rus, M.A.A., Myhre, P.L., Boghdady, G.Y., Corfu, F., in press. U–Pb TIMS age constraints on the evolution of the Neoproterozoic Meatiq Gneiss Dome, Eastern Desert, Egypt. *International Journal of Earth Sciences (Geol Rundsch)*.
- Be'eri-Shlevin, Y., 2008. The origin and evolution of Neoproterozoic magmatism in the northern Arabian-Nubian Shield (Sinai Peninsula, Egypt and southern Israel): evidence from stable and radiogenic isotope record. Unpublished Ph.D. thesis, Ben-Gurion University, Israel. 134 pp.
- Be'eri-Shlevin, Y., Katzir, Y., Whitehouse, M.J., 2008. Contribution of pre Pan-African crust to the formation of the northernmost Arabian-Nubian Shield: evidence from SIMS U–Pb dating of zircon. 33rd International Geological Congress. Norway, Oslo. August 2008.
- Be'eri-Shlevin, Y., Katzir, Y., Whitehouse, M.J., 2009. Post-collisional tectono-magmatic evolution in the northern Arabian Nubian Shield (ANS): time constraints from ion-probe U–Pb dating of zircon. *Journal of the Geological Society of London* 166, 1–15.
- Bentor, Y.K., 1985. The crustal evolution of the Arabian-Nubian Massif with special reference to the Sinai Peninsula. *Precambrian Research* 28, 1–74.
- Bentor, Y.K., Eyal, M., 1987. The Geology of Southern Sinai, its Implication for the Evolution of the Arabian-Nubian Massif Volume 1: Jebel Sabbagh Sheet. Israel Academy of Sciences and Humanities, Jerusalem.
- Beyth, M., Stern, R., Altherr, R., Kröner, A., 1994. The late Precambrian Timna igneous complex, Southern Israel: evidence for comagmatic-type sanukitoid monzodiorite and alkali granite magma. *Lithos* 31, 103–124.
- Bielski, M., 1982. Stages in the evolution of the Arabian-Nubian massif in Sinai. Unpublished Ph.D. thesis, Hebrew University of Jerusalem. 155 pp.
- Blasband, B., Brooijmans, P., Dirks, P., Visser, W., White, S., 1997. A Pan-African core complex in the Sinai, Egypt. *Geologie en Mijnbouw* 73, 247–266.
- Bonin, B., 2007. A-type granites and related rocks: evolution of a concept, problems and prospects. *Lithos* 97, 1–29.
- Cosca, M.A., Shimron, A., Caby, R., 1999. Late Precambrian metamorphism and cooling in the Arabian-Nubian Shield: petrology and  $^{40}\text{Ar}/^{39}\text{Ar}$  geochronology of metamorphic rocks of the Elat area (southern Israel). *Precambrian Research* 98, 107–127.
- Cavosie, A.J., Valley, J.W., Wilde, S.A., EIMF, 2006. Correlated microanalysis of zircon: Trace element,  $\delta^{18}\text{O}$ , and U–Th–Pb isotopic constraints on the igneous origin of complex >3900 Ma detrital grains. *Geochimica et Cosmochimica Acta* 70, 5601–5616.
- Eiler, J.M., 2001. Oxygen isotope variations of basaltic lavas and upper mantle rocks. In: Valley, J.W., Cole, D.R. (Eds.), *Stable Isotope Geochemistry: MSA Reviews in Mineralogy series*, vol. 43, pp. 319–364.
- El-Shafei, M.K., Kusky, T.M., 2003. Structural and tectonic evolution of the Neoproterozoic Feiran-Solaf metamorphic belt, Sinai Peninsula: implications for the closure of the Mozambique Ocean. *Precambrian Research* 123, 269–293.
- Eyal, Y., 1980. The geological history of the Precambrian metamorphic rocks between Wadi Twaiba and Wadi Um-Mara, NE Sinai. *Israel Journal of Earth Sciences* 29, 53–66.
- Eyal, M., Bartov, Y., Shimron, A.E., Bentor, Y.K., 1980. Sinai geological map 1:500,000 scale. Geological Survey of Israel, Jerusalem.
- Eyal, Y., Eyal, M., Kröner, A., 1991. Geochronology of the Elat Terrain metamorphic basement, and its implication for crustal evolution of the NE part of the Arabian-Nubian Shield. *Israel Journal of Earth Sciences* 40, 5–16.
- Eyal, M., Litvinovsky, B.A., Katzir, Y., Zanzilevich, A.N., 2004. The Pan-African high-K calc-alkaline peraluminous Elat granite of southern Israel: geology, geochemistry and petrogenesis. *Journal of African Earth Sciences* 40, 115–136.
- Garfunkel, Z., 1999. History and paleogeography during the Pan-African orogen to stable platform transition: reappraisal of the evidence from Elat area and northern Arabian-Nubian Shield. *Israel Journal of Earth Sciences* 48, 135–157.
- Halpern, M., Tristan, N., 1981. Geochronology of the Arabian-Nubian Shield in southern Israel and eastern Sinai. *Journal of Geology* 89, 639–648.
- Hargrove, U.S., Stern, R.J., Kimura, J.-I., Manton, W.I., Johnson, P.R., 2006. How juvenile is the Arabian-Nubian shield? Evidence from Nd isotopes and pre-Neoproterozoic inherited zircon in the Bi'r Umq suture zone, Saudi Arabia. *Earth and Planetary Science Letters* 252, 308–326.
- Hoskin, P.W.O., Schaltegger, U., 2003. The composition of zircon and igneous and metamorphic petrogenesis. In: Hanchar, J., Hoskin, P. (Eds.), *Zircon: MSA Reviews in Mineralogy and Geochemistry*, vol. 53, pp. 27–62.
- Jarrar, G., Stern, R.G., Saffarini, H., Al-Zubi, 2003. Late- and post-orogenic Neoproterozoic intrusions of Jordan: implications for crustal growth in the northernmost segment of the East African Orogen. *Precambrian Research* 123, 295–319.
- Jarrar, G., Saffarini, G., Baumann, A., Wachendorf, H., 2004. Origin, age and petrogenesis of Neoproterozoic composite dikes from the Arabian-Nubian Shield, SW Jordan. *Geological Journal* 39, 157–178.
- Jarrar, G.H., Manton, W.I., Stern, R.J., Zachmann, 2008. Late Neoproterozoic A-type granites in the northernmost Arabian-Nubian Shield formed by fractionation of basaltic melts. *Chemie der Erde* 68, 295–312.
- Katz, O., Avigad, D., Matthews, A., Heimann, A., 1998. Precambrian metamorphic evolution of the Arabian-Nubian Shield in the Roded area, southern Israel. *Israel Journal of Earth Sciences* 47, 93–110.
- Katz, O., Beyth, M., Miller, N., Stern, R., Avigad, D., Basu, A., Anbar, A., 2004. A late Neoproterozoic (~630 Ma) high-magnesium andesite suite from southern Israel: implications for the consolidation of Gondwanaland. *Earth and Planetary Science Letters* 218, 275–290.
- Katzir, Y., Litvinovsky, B.A., Jahn, B.M., Eyal, M., Zanzilevich, A.N., Vapnik, Ye., 2006. Four successive episodes of Late Pan-African dikes in the central Elat area, southern Israel. *Israel Journal of Earth Sciences* 55, 69–93.
- Katzir, Y., Eyal, M., Litvinovsky, B.A., Jahn, B.M., Zanzilevich, A.N., Valley, J.W., Beeri, Y., Pelly, I., Shimshilashvili, E., 2007a. Petrogenesis of A-type granites and origin of vertical zoning in the Katharina pluton, area of Gebel Mussa (Mt. Mosses), Sinai, Egypt. *Lithos* 95, 208–228.
- Katzir, Y., Litvinovsky, B.A., Jahn, B.M., Eyal, M., Zanzilevich, A.N., Valley, J.W., Vapnik, Ye., Beeri, Y., Spicuzza, M.J., 2007b. Interrelations between coeval mafic and A-type silicic magmas from composite dykes in a bimodal suite of southern Israel, northernmost Arabian-Nubian Shield: geochemical and isotope constraints. *Lithos* 97, 336–364.
- Kennedy, A., Johnson, P.R., Kattan, F.H., 2004. SHRIMP geochronology in the northern Arabian Shield, part 1: data acquisition. Saudi Geological Survey Open File Report SGS-OF-2004-11, p. 28.
- Kolodner, K., Avigad, D., McWilliams, M., Wooden, J.L., Weissbrod, T., Feinstein, S., 2006. Provenance of north Gondwana Cambrian-Ordovician sandstone: U–Pb SHRIMP dating of detrital zircons from Israel and Jordan. *Geological Magazine* 143, 367–391.
- Kolodner, K., 2007. The provenance of the siliciclastic section in Israel and Jordan: U–Pb dating of detrital zircons. Unpublished Ph.D. thesis, Hebrew University of Jerusalem, Israel. 133 pp.
- Kröner, A., Eyal, M., Eyal, Y., 1990. Early Pan-African evolution of the basement around Elat, Israel, and Sinai Peninsula revealed by single-zircon evaporation dating, and implications for crustal accretion rates. *Geology* 18, 545–548.
- Kröner, A., Krüger, J., Rashwan, A.A.A., 1994. Age and tectonic setting of granitoid gneisses in the Eastern Desert of Egypt and south-west Sinai. *International Journal of Earth Sciences (Geol Rundsch)* 83, 502–513.
- Matthews, A., Reymer, A.P.S., Avigad, D., Cochlin, J., Marco, S., 1989. Pressures and temperatures of Pan-African high grade metamorphism in the Eilat Association, N.E. Sinai. *Israel Journal of Earth Sciences* 38, 1–17.
- Meert, J.G., 2003. A synopsis of events related to the assembly of eastern Gondwana. *Tectonophysics* 362, 1–40.
- Moghazi, A.M., Anderson, T., Oweiss, G.A., El Bousely, A.M., 1998. Geochemical and Sr–Nd isotopic data bearing on the origin of Pan-African granitoids in the Kid area, southeast Sinai, Egypt. *Journal of the Geological Society of London* 155, 697–710.
- Morag, N., Avigad, D., Kolodner, K., Belousova, E., Ireland, T., Harlavan, Y., 2007. Hf-in-zircon perspective on crustal growth and recycling in the Arabian Nubian Shield. *Goldschmidt Conference Abstracts*, Cologne, p. A685. August 2007.
- Moussa, E.M.M., Stern, R.J., Manton, W.I., Ali, K.A., 2008. SHRIMP zircon dating and Sm/Nd isotopic investigations of Neoproterozoic granitoids, Eastern Desert, Egypt. *Precambrian Research* 160, 341–356.
- Mushkin, A., Navon, O., Halitz, L., Heimann, A., Woerner, G., Stein, M., 1999. Geology and geochronology of the Amram Massif, Southern Negev Desert, Israel. *Israel Journal of Earth Sciences* 49, 179–193.
- Mushkin, A., Navon, O., Halitz, L., Heimann, A., Hartmann, G., Stein, M., 2003. The petrogenesis of A-type magmas from the Amram Massif, southern Israel. *Journal of Petrology* 44, 815–832.
- Peck, W.H., King, E.M., Valley, J.W., 2000. Oxygen isotope perspective on Precambrian crustal growth and maturation. *Geology* 28, 363–366.
- Reymer, A., Schubert, G., 1986. Rapid growth of major segments of continental crust. *Geology* 14, 299–302.
- Shimron, A.E., 1984. Evolution of the Kid Group, southeast Sinai Peninsula: thrusts, mélanges, and implications for accretionary tectonics during the Proterozoic of the Arabian-Nubian Shield. *Geology* 12, 242–247.
- Stacey, J.S., Agar, R.A., 1985. U–Pb isotopic evidence for the accretion of a continental micro-plate in the Zalm region of the Saudi-Arabian Shield. *Journal of the Geological Society of London* 142, 1189–1203.
- Stein, M., 2003. Tracing the plume material in the Arabian-Nubian Shield. *Precambrian Research* 123, 223–234.

- Stein, M., Goldstein, S., 1996. From plume head to continental lithosphere in the Arabian-Nubian Shield. *Nature* 382, 773–778.
- Stern, R.J., 1985. The Najd Fault System, Saudi Arabia and Egypt: a late Precambrian rift related transform system. *Tectonics* 4, 497–511.
- Stern, R.J., 1994. Arc assembly and continental collision in the Neoproterozoic East African Orogen: implications for the consolidation of Gondwanaland. *Annual Reviews of Earth and Planetary Sciences* 22, 319–351.
- Stern, R.J., 2002. Crustal evolution in the East African Orogen: a neodymium isotopic perspective. *Journal of African Earth Sciences* 34, 109–117.
- Stern, R.J., Hedge, C.E., 1985. Geochronologic and isotopic constraints on Late Proterozoic crustal evolution in the Eastern Desert of Egypt. *American Journal of Science* 285, 97–127.
- Stern, R.J., Manton, W.I., 1987. Age of Feiran basement rocks, Sinai: implications for late Precambrian crustal evolution in the northern Arabian-Nubian Shield. *Journal of the Geological Society, London* 144, 569–575.
- Stoeser, D.B., Camp, V.E., 1985. Pan-African microplate accretion of the Arabian Shield. *Geological Society of America Bulletin* 96, 817–826.
- Stoeser, D.B., Frost, C.D., 2006. Nd, Pb, Sr, and O isotopic characterization of Saudi Arabian Shield terranes. *Chemical Geology* 226, 163–188.
- Sultan, M., Chamberlin, K.R., Bowring, S.A., Arvidson, R.E., Abuzied, H., El Kaliouby, B., 1990. Geochronologic and isotopic evidence for the involvement of pre Pan-African crust in the Nubian Shield, Egypt. *Geology* 18, 761–764.
- Taylor, H.P., 1986. Igneous rocks: II. Isotopic case studies of circumpacific magmatism. In: Valley, J.W., Taylor, H.P., O'Neil, J.R. (Eds.), *Stable Isotopes: MSA Reviews in Mineralogy*, vol. 16, pp. 273–317.
- Valley, J.W., 2003. Oxygen isotopes in zircon. In: Hanchar, J., Hoskin, P. (Eds.), *Zircon: MSA Reviews in Mineralogy and Geochemistry*, vol. 53, pp. 343–385.
- Valley, J.W., Kinny, P.D., Schulze, D.J., Spicuzza, M.J., 1998. Zircon megacrysts from kimberlite: oxygen isotope variability among mantle melts. *Contributions to Mineralogy and Petrology* 133, 1–11.
- Valley, J.W., Kitchen, N., Kohn, M.J., Niendorf, C.R., Spicuzza, M.J., 1995. UWG-2, a garnet standard for oxygen isotope ratio: strategies for high precision and accuracy with laser heating. *Geochimica et Cosmochimica Acta* 59, 5223–5231.
- Valley, J.W., Lackey, J.S., Cavosie, A.J., Clechenko, C.C., Spicuzza, M.J., Basei, M.A.S., Bindeman, I.N., Ferreira, V.P., Sial, A.N., King, E.M., Peck, W.H., Sinha, A.K., Wei, C.S., 2005. 4.4 billion years of crustal maturation: oxygen isotopes in magmatic zircon. *Contributions to Mineralogy and Petrology* 150, 561–580.
- Wei, C.S., Zheng, Y.F., Zhao, Z.F., Valley, J.W., 2002. Oxygen and neodymium isotope evidence for recycling of juvenile crust in northeast China. *Geology* 30, 375–378.